The digital terrain model in the computational modelling of the flow over the Perdigão site: the appropriate grid size

authored by
José M. L. M. Palma, Carlos A. M. Silva, Vitor M. C. Gomes, Alexandre Silva Lopes, Teresa Simões, Paula Costa, and Vasco T. P. Batista
Submitted for publication in the *Wind Energy Science*
https://doi.org/10.5194/wes-2019-96

Reply to comments by Reviewer 1 (M. Paul van der Laan, DTU Wind Energy)

The authors investigate the impact of different terrain models with different resolutions on atmospheric flow simulations of the Perdigão site. The authors recommend a horizontal threshold resolution of 40 m. The authors define a *threshold resolution*, as the resolution beyond which the model quality deteriorated quickly, but below which no significant improvement in modelling results was observed. The article is well written, follows a good structure and includes a lot of useful technical information about the Perdigão site and related terrain models. However, I have two main comments about the article.

My main concern about using a *threshold resolution* is the fact that is not general, while it is the main objective of the article to find such a resolution, as the authors mention on Page 3, Line 68. The required resolution of the terrain map and flow model mesh are dependent on the quantities of interest. For example, one could be interested in the integrated drag force of the entire terrain, which might require a less strict level of refinement compared to a specific profile of a flow quantity near the ground and in the lee of a steep hill. This means that the concept of a threshold resolution, as mentioned in the introduction is not general, but it depends on the quantity of interest. In addition, the chosen flow model can also influence the required resolution. This is the reason why every article including a new flow model setup needs to be verified by a grid refinement study.

REPLY (First/Main concern or comment):

1. As shown by the title, our main concern is the terrain modelling, not the flow modelling or the flow results. First, we wanted to know to what extent the resolution of the digital terrain model (DTM) affects the terrain modelling and, second, how the terrain modelling affects the flow results.
2. The first (assessment of resolution on terrain modelling, section 4) was carried out by comparing terrain modelling results (terrain elevation and slope) on meshes of different resolutions (80, 40 and 20 m) based on two DTMs of different resolution (SRTM and Mil) against terrain modelling results on meshes based on a higher resolution (ALS) DTM.
    - This analysis was made on the basis of terrain properties (or attributes) of interest to atmospheric flow modelling; i.e. terrain elevation and terrain slope. Because these two are the most important and for the sake of simplicity, land coverage (roughness) was assumed constant.

3. The second (impact of terrain model resolution on flow model results, section 5) was carried out by analysing the flow results based on those meshes and DTMs.
   - This analysis was based on the vertical profiles of wind speed, wind direction and turbulent kinetic energy at three locations, and flow pattern at two transects. These variables and the locations were selected because of their importance in wind energy and sensitivity to the mesh resolution.
4. About *threshold resolution* and flow model results we note the following:
   (a) One must distinguish between the *threshold resolution* in the context of the terrain model and in the context of the flow model. The former is much simpler, independent of the flow model and was dealt with in full in section 4.
   (b) In the case of the flow model results, the *threshold resolution* depends on the flow model (e.g., discretization techniques) and for the same flow model will depend of the parameters of a given run (domain size, boundary conditions, mesh resolution along any direction, etc.).
   (c) The mesh is comprised by the horizontal mesh describing the terrain shape (the digital terrain model), often a terrain-following coordinate system, and the mesh along the vertical.
   (d) There are guidelines for setting the vertical mesh, namely the distance between the first grid node and the ground, but there are no guidelines for how fine the horizontal mesh should be.
   (e) The comment that *threshold resolution* is not general and depends on the flow model, suggests that our conclusions cannot be generalised. We are aware of that, nevertheless, we consider ours a useful work, because we are not expecting the resolution requirements (or the *threshold resolution*) to be much different, given the similarities among the available models.

My second main comment is that not all conclusions are motivated by the presented results because the grid errors of vertical profiles of wind speed, wind direction and turbulent kinetic energy are not directly shown and not clearly quantified.

> REPLY (Second main comment):
> We do not understand this comment. The vertical profiles of wind speed, wind direction and turbulent kinetic energy are shown (Figures 14, 15 and 16) for all meshes (80, 40 and 20 m) and DTMs (SRTM, Mil and ALS) and the errors quantified (see RMSE in Tables 6, 7 and 8).

I have listed related and additional main and minor comments below, which need to [be] addressed in order to consider a publication in Wind Energy Science.

Main comments

1. Page 3, Line 54: What is meant *by terrain attributes and topographic meaning in Deng et al. (2007) indicates that the mesh resolution can change not only terrain attributes in*

specific points but also the topographic meaning of attributes at each point. Do you mean roughness length? Please clarify.

REPLY:
Terrain attributes are elevation, slope, plan and profile curvature, and topographic wetness index, as defined in lines 45 and 46. For instance, Deng et al. (2007) listed and evaluated six terrain attributes (slope, plan curvature, profile curvature, north-south slope orientation, east-west slope orientation, and topographic wetness index) as a function of DTM resolution.

The terrain attributes of interest to atmospheric flow modelling are terrain elevation, terrain slope and terrain or land coverage, i.e. roughness.

2. What do you mean by *switched on 1 sec registration after assistance by the Portuguese National Mapping Agency*? Do you mean a sampling frequency of 1 Hz?

REPLY:
Yes.

3. Section 5.1.1: I do not understand that you k profile is varying with height. If you use a log profile for the streamwise velocity at the inlet, then I assume that you are modelling an atmospheric surface layer, which is represents a constant k value, as discussed by Richards and Hoxey (1993). In addition, if you model a boundary layer height by simply capping it above a certain height, how do you make sure that such an inflow profile is in balance with an empty (flat terrain) flow domain? If the inflow profile is not in balance with your RANS model, then the results at area of interest are dependent on the distance of inflow boundary to the area of interest, which is highly unfavorable.

REPLY:
The distance between the inlet boundary and the area of interest was identical in all simulations.

4. Page 6, Line 157: You mention *The slope, ... varies between 21.08º and 45.09º, always above the threshold for flow separation (Wood, 1995).* However, flow separation also depends on the roughness length and atmospheric conditions as turbulence intensity and atmospheric stability. So an attached flow could exist for a hill with a 21^o slope if the conditions allow it. Wood (1995) only looked at neutral atmospheric conditions. Therefore, I think you rephrase your statement that flow separation is likely to occur for the site your are investigating.

REPLY:
Changed, as suggested. The new version reads:
The slope ($S = |atan(h_{SW,NE}/2)|/\ell_{SW,NE}$), also on a 20 m *grid varies between* 21.08° *and* 45.09°*, always above the threshold for flow separation under neutral conditions (Wood, 1995).*

5. Page 16-17, Lines 272-274: You mention that results from 20 and 40 m meshes yield similar results and appear to be accurate enough for computational modelling of atmospheric flow

over Perdigão based on Figure 12, using the reversed flow regions. Please clarify *appear to be accurate enough* by quantifying the differences in order to motivate your statement. You could also remove this statement and quantify the differences in Section 5.4.

REPLY:
The text was rewritten and experimental values by Menke et al. (2019) included.

6. Figures 14-16: I would not plot the simulation results of the different meshes together with the measurements in the same figure in order to separate the grid refinement study (model verification) from the model validation. I would also remove the statement on Page 19, Lines 286-287: *For some reason, in the valley the best agreement with the experimental data occurred in the case of the coarser meshes.* (A common mistake in literature is to choose a coarser grid because it compares better with measurements and I would recommended that you do not suggest the reader to do so.) If you would like to include a model validation, you could make separate plots of the chosen grid size (or finest grid size) for each terrain input model and measurements. In addition, have you tried to normalize the measurements and CFD results of wind speed and TKE with their local friction velocity u_{*0}?

   REPLY:
   Computational and experimental results in the same figure are necessary to show how similar or different they are. Plots of the chosen grid size for each terrain input would increase the number of figures. By plotting the results at the valley we are not suggesting that the reader should choose the coarser meshes; cases like these, where coarser meshes provide better agreement with experimental data, are not so uncommon. The text was rewritten.

7. Page 19, Lines 288-290: You mention: *As a whole, results depend more on the resolution than on the DTM and at least a resolution of 40 m is required. Differences between the computational results on 20 and 40 m resolution meshes are minor and within the uncertainty of computational modelling.* This statement is not sufficiently shown in Figure 14-16. I would suggest to (also) plot the differences between the inflow profiles in percentages as function of height, with respect to the reference simulations. This should provide a more clear presentation of the differences between the simulations compared to the RMSE values of Tables 6-8. You can then conclude that the grid error in (for example) wind speed at the reference locations, at a certain height (e.g. around a typical onshore wind turbine hub height) is x% and then it is easier to quantify the impact of grid resolution and terrain model on a wind resource assessment.

   REPLY:
   First, we do not see how the suggested representation can provide a clearer presentation of the differences between the simulations. Second, this type of representation (in absolute values) gives us an idea of the uncertainty for each variable in its own absolute values.

8. Page 20, Line 304: I could not find the second statement of the conclusion elsewhere in the article: *Only meshes based on the ALS have the ability to reproduce the smaller scales between 10 and 100 m.* Please remove the statement from the conclusion or motivate it in the article.

REPLY:
This is related to Figure 11 and section 4.4.

9. Page 21, Lines 320-327: The conclusions made here are not motivated by the results presented in the article.

   (a) I do not agree with the concept of a threshold resolution because it depends on both the applied flow solver and quantity of interest. You can either remove it or reduce the statement by writing that required resolution only applies to your investigated quantities of interest and the chosen flow solver. This also applies to the abstract, title and motivation.

   REPLY:
   Please, refer to our first comment on terrain attributes and objective of the study. Note also that the title is already a long one and the conditions under which our study was carried out are described in full in the abstract, including the flow solver.

   (b) Statements 2 and 3 should be motivated with plots showing the grid error in terms of percentages, as mention previously.

   REPLY:
   This matter is the subject of section 4, thoroughly illustrated by Figures 6 to 11, and Tables 3 and 4. The statement (2) that SRTM should be restricted to far away regions is supported by Table 3, where it can be seen that the absolute error of SRTM is equal to 10 m. Statement 3 is a final recommendation and message of the article, where we say, please use this dataset (ALS) and meshes of at least 40 m horizontal resolution.

Minor comments

1. Section 1.1: It is more common to use a past tense instead of a present tense when referring to literature. (For example on Page 3, Line 59: develops → developed.)

   REPLY:
   You are right. The whole section 1.1 was revised.

2. Page 3, Line 64: Please rephrase *..the flow with the sharp edge..*, because it is the terrain model geometry that has a sharp edge, not the flow.

   REPLY:
   It now reads *the cliff with the sharp edge*

3. Page 15, Line 253: I would abbreviate Reynolds-averaged Navier-Stokes as RANS, which is more common. In addition, you forgot to define RANS.

   REPLY:
   The acronym was removed, because it was not used.

4. Page 15, Line 253: I would write the two equation $k-\varepsilon$ model with k instead of κ, as κ is commonly used as the Von Karman constant and you also use k as the turbulent kinetic energy.

   REPLY:
   This was a misspelling. It should be as in line 247.

5. Not all reported values need to reported fully. For example, you could report 22071075 m^2 as 22.1×10^6 m^2 (Page 4, Line 79) and 993198375 as 10^9 approximately (Page 4, Line 79), this also applies elsewhere in the article.

   REPLY:
   These are detailed technical specifications, usually found in aerial topographical surveys, useful to readers in this area.

6. Page 6, Line 33: I would rephrase the parallelism between the two ridges.

   REPLY:
   We do not see anything wrong with this sentence.

7. Page 7, Line 145: Do you know the distances between the ridges in cm? If not, I would remove the two zeros.

   REPLY:
   Yes, you are right.

References

Y. Deng, J. P. Wilson, and B. O. Bauer. DEM resolution dependencies of terrain attributes across a landscape. *International Journal of Geographical Information Science*, 21(2):187–213, January 2007. ISSN 1365-8816, 1362-3087. doi: 10.1080/13658810600894364. URL `http://www.tandfonline.com/doi/abs/10.1080/13658810600894364`.

R. Menke, N. Vasiljević, J. Mann, and J. K. Lundquist. Characterization of flow recirculation zones at the Perdigão site using multi-lidar measurements. *Atmospheric Chemistry and Physics*, 19(4):2713–2723, March 2019. ISSN 1680-7316. doi: 10.5194/acp-19-2713-2019. URL `https://www.atmos-chem-phys.net/19/2713/2019/`.

P.J Richards and R.P. Hoxey. Appropriate boundary conditions for computational wind engineering models using the $k-\varepsilon$ turbulence model. *Journal of Wind Engineering and Industrial Aerodynamics*, 46-47:145–153, August 1993. ISSN 0167-6105. doi: 10.1016/0167-6105(93)90124-7. URL `http://www.sciencedirect.com/science/article/B6V3M-4847B4C-K/2/6f6fa2909840b477522ec73bd33ba220`.

N. Wood. The onset of separation in neutral, turbulent flow over hills. *Boundary-Layer Meteorology*, 76(1-2):137–164, 1995. ISSN 0006-8314. doi: 10.1007/BF00710894. URL `http://www.springerlink.com/content/v2412rh223072568/`.

The digital terrain model in the computational modelling of the flow over the Perdigão site: the appropriate grid size

authored by
José M. L. M. Palma, Carlos A. M. Silva, Vitor M. C. Gomes, Alexandre Silva Lopes, Teresa Simões, Paula Costa, and Vasco T. P. Batista
Submitted for publication in the *Wind Energy Science*
https://doi.org/10.5194/wes-2019-96

Reply to comments by Reviewer 2 (Anonymous)

The paper addresses the important problem of the numerical model setup for simulations of the wind over two parallel ridges at the Perdigão site, the area of interest during the intensive observational campaign of the New European Wind Atlas project.

The introduction is too long, given that the problem is quite a straightforward one: the numerical model resolution is sufficient when further refinement no longer affects the results. This is often ignored by necessity due to computational cost, and compromises are generally accepted if the results are still applicable after validation. So the goal of this interesting and relevant paper could be elegantly achieved by presenting a clear and comprehensive overview of the resolution requirements, so that future simulations of this highly studied area can easily be set up and evaluated with respect to the terrain and grid resolution.

> REPLY:
> We do not understand the comment. The introduction is two pages long. This is not a grid refinement study as usually in a computational fluid dynamics study. We are concerned mainly with the resolution of the digital terrain model. These are matters that go beyond computational fluid dynamics and have been dealt with in other disciplines, namely geomorphology. We are of the opinion that mainly in complex terrain, the accuracy of terrain model should precede the CFD three-dimensional grid and this is the message that we try to convey in section 1. Furthermore, the final message is that in Perdigão (and any complex site) the publicly available databases (e.g. SRTM, ASTER) are not accurate enough.

I would recommend that the paper is published after revision, addressing the specific comments below.

Specific comments:

L23: It is unclear what is meant with the resolution of the measuring equipment. Perhaps density would be a better word.

> REPLY:
> The proximity between measuring stations is very low. It reads now *on par with the resolution provided by such a large number of measuring equipment within a small region.*

L24: Please provide the geographic coordinates in WGS84 at this stage, and the equivalent in UTM. It is acceptable to use UTM later in the text.

REPLY:
Yes.

L33: The SRTM terrain resolution is 1" (24 m) but in the conclusions it is considered inadequate, in spite that the 40 m resolution is recommended as a minimum. Please comment.

REPLY:
For meshes with identical horizontal resolution (Figures 6 and 7), both SRTM and Mil yield higher RMSE of terrain elevation than meshes based on ALS. Terrain elevation (z_{Max}, Table 3) and slope (S_{Max}, Table 4) are higher for meshes based on ALS. It is not just a question of horizontal resolution, but the RMSE of terrain elevation of both SRTM and Mil. The abstract says it all.

L58: The threshold resolution is not a concept, but a requirement in numerical modelling. It is often ignored by necessity due to computation cost.

REPLY:
No comment.

L80: 22 square km would be easier to understand than 22 million square meters.

REPLY:
No comment.

L79,84: What is Blom TopEye? TPDS? Please supply a reference or description.

REPLY:
Blom[1] is the largest company in Europe, specialized on topographic laser ranging and scanning (Mallet and Bretar, 2009). TPDS and TASQ are acronyms of software by Blom. The information in the first four paragraphs of section 2.1 is technical information related to the lidar scanning.

L81: This is an impressive number of points in the cloud, but does it have any relevance? Please remove.

REPLY:
This information is generally provided in all laser scanning surveys and is essential for determining the horizontal resolution.

[1] http://www.skgeodesy.sk/files/slovensky/ugkk/medzinarodna-spolupraca/bilateralna-spolupraca/norSirotek-2-Bratislava.pdf

L83-89: This paragraph is very hard to comprehend. Please reformulate.

REPLY:
The text was rewritten.

L94, Figure 1: please display the two images in the same projection

REPLY:
Our apologies, we were unable to display the images in the same projection, due to different software used to draw either image.

L96: Table ?? ?

REPLY:
Reference to a missing table was removed.

L135: It is important to remember that the concept of two-dimensionality quickly breaks in the case of atmospheric flows, i.e. as soon as not all the forces acting on an air parcel are aligned with the 2D plane.

REPLY:
Yes, but that does not invalidate our statement, which is from the strictly geometrical point of view, given the high length to width ratio.

L146: It is inappropriate to use anything more precise than integer meters when describing terrain altitude with regard to atmospheric modelling. The same for geographic coordinates, for example in Table 1, especially since the highest data resolution is 2 m.

REPLY:
The 2 m resolution is the horizontal resolution, because this was the finest mesh generated from the lidar data. However, it is acknowledged that the vertical and planimetric accuracy of the airborne laser scanning are lower than 0.1 m and 0.4 cm (Mallet and Bretar, 2009). Geographic coordinates are now in metre (Table 1) and terrain elevation in decimetre (Tables 1 and 2).

L228-233, Section 5: It is unlikely that the atmospheric conditions at 22 UTC are neutral and stationary, as the simulation setup assumes. It is also unclear whether the authors are aware that the conditions might not be neutral and stationary, yet they proceed with the analysis because the referred publications have established the opposite? Please clarify by including the measurements of relevant parameters.

REPLY:
Yes, we are aware. That was the reason why we selected the 30 minutes averaged between 22:09–22:39 UTM on 4 May 2017. Because from the analysis of the 45 days of the IOP (Intensive operation period), this was a period during which stationarity conditions could be assumed. The reference (Carvalho, 2019), supporting our statement, is publicly available and the data was plotted in a way that shows the deviation from stationarity. The text was rewritten and information on stratification was also provided.

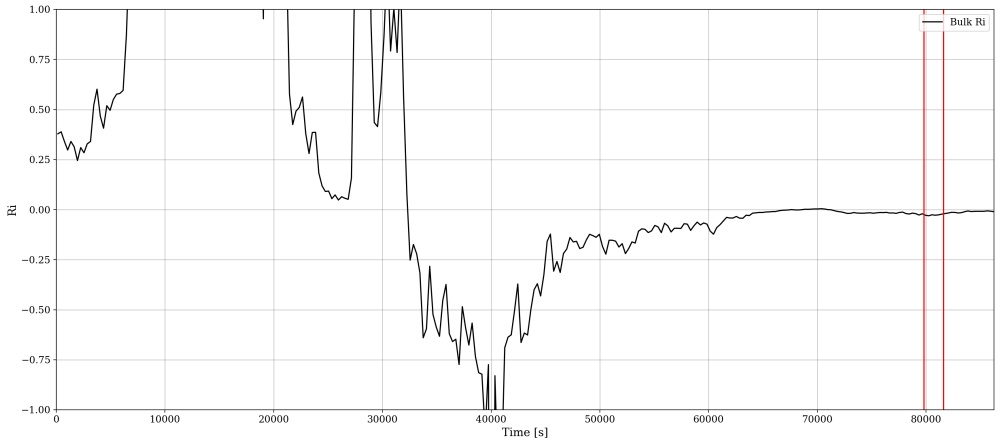

Figure 1: Bulk Richardson number

L246-250: Is it justifiable to use uniform roughness for this simulation? Have you performed any sensitivity analyses if the sufficient resolution threshold changes when non-uniform roughness is used?

REPLY:
It is justifiable only to reduce the number of variables influencing the problem. Our main objective was to assess the resolution required for the digital terrain model. There was no sensitivity analysis on the effect of non-uniform roughness; this will be the subject of future publications, as stated in the paper. The land coverage at Perdigão is a heterogeneous distribution of eucalyptus and pine trees and will require an approach different from simple characteristic roughness.

L250: Does the impact of the first node height show any convergence, like it is the case for the horizontal resolution? You state that this is worthy of further studies, whereas this is the very study where this should be evaluated.

REPLY:
The impact of the first node height would bring to the discussion other aspects of

computational modelling, beyond the scope of the present paper, focused strictly on the digital terrain model and how accurate the description of the terrain surface must be. A large proportion of Perdigão area is covered by trees, a canopy model will be required to resolve these regions and the first node height is not the only parameter to take into account when using canopy models Lopes da Costa et al. (2006) Silva Lopes et al. (2013).

L278, Figures 12,13: It is not clear what in these figures exactly illustrates the impact of mesh resolution. Are we supposed to see the differences in the insets? Please provide more information in the captions and some discussion about the figures in the text.

REPLY:
Figures 12 and 13 were redrawn and the lines in the insets were corrected.

L282: The statement how too high z_0 and u_* yield a high loss of momentum is probably badly formulated.

REPLY:
The text was rewritten.

L291, Figures 14, 15, 16: There are several revealing features in the figures, but only the absolute wind speed, and to some extent the TKE, receive any discussion. The diverging wind speed in the higher altitudes in Figure 15a is particularly interesting. The legend is hard to read.

REPLY:
Figures 14, 15 and 16 were redrawn and the text rewritten.

L294: Please clarify what is meant by "... where a pattern similar to the slope (Table 4) can be observed."

REPLY:
The text was rewritten.

L294: Is the RMSE calculated over all the points in the vertical where the measurements are available? The relevance of this statistical measure in a situation where the basic characteristics of the two datasets disagree quite fundamentally (e.g. the TKE at the tower 20/tse04, Figure 14) is probably questionable.

REPLY:
No, the RMSE is calculated over the whole profile; it is the RMSE measured against the results on the 20 m resolution mesh (ALS). It is questionable, but once we use this indicator for one variable it should be used for all others.

L304: This conclusion 1. is very categorical, while not entirely based on presented facts. At the resolution of 40 m, which is suggested as sufficient for Perdigão, the RMSE for the SRTM-based simulation is not systematically larger than of the other two datasets; in fact, it can be seen that in terms of RMSE for the 40 m resolution the SRTM-based simulations often have the lowest RMSE (Tables 6, 7, 8).

REPLY:
This conclusion is based on the SRTM ability to replicate the ALS data. It is not based on the comparison of flow results using computational meshes from different DTM sources. This conclusion is based on section 4, namely Figures 6 to 11, and Tables 3 and 4, and is based on the ability of the SRTM data to replicate the terrain elevation and slope as measured by the airborne laser scanning (2015).

Please note that the conclusions are organized into three groups: related to the DTM sources (numbered from 1 to 5), flow model (numbered from 1 to 3) and the final recommendations (numbered from 1 to 3).

References

J. P. D. B. Carvalho. Stationarity periods during the Perdigão campaign. Master's thesis, Faculty of Engineering of the University of Porto, 2019. URL `https://repositorio-aberto.up.pt/bitstream/10216/122036/2/348346.pdf`.

J. C. Lopes da Costa, F.A. Castro, J.M.L.M. Palma, and P. Stuart. Computer simulation of atmospheric flows over real forests for wind energy resource evaluation. *Journal of Wind Engineering and Industrial Aerodynamics*, 94:603–620, 2006. doi: 10.1016/j.jweia.2006.02.002. URL `https://www.sciencedirect.com/science/article/pii/S0167610506000328`.

C. Mallet and F. Bretar. Full-waveform topographic lidar: State-of-the-art. *ISPRS Journal of Photogrammetry and Remote Sensing*, 64(1):1–16, January 2009. ISSN 0924-2716. doi: 10.1016/j.isprsjprs.2008.09.007. URL `http://www.sciencedirect.com/science/article/pii/S0924271608000993`.

A. Silva Lopes, J.M.L.M. Palma, and J. Viana Lopes. Improving a two-equation turbulence model for canopy flows using large-eddy simulation. *Boundary-Layer Meteorology*, 149(2): 231–257, November 2013. ISSN 0006-8314, 1573-1472. doi: 10.1007/s10546-013-9850-x. URL `http://link.springer.com/article/10.1007/s10546-013-9850-x`.

The digital terrain model in the computational modelling of the ~~flow~~ flow over the Perdigão site: the appropriate grid size

José M.L.M Palma[1], Carlos A.M. Silva[1], Vitor M.C. Gomes[1], Alexandre Silva Lopes[1], Teresa Simões[2], Paula Costa[2], and Vasco T.P. Batista[1]

[1]Faculty of Engineering of the University of Porto (FEUP), Mechanical Engineering Department, Rua Dr. Roberto Frias, s/n, 4200-465 Porto, Portugal
[2]National Laboratory of Energy and Geology (LNEG), Estrada da Portela, Bairro do Zambujal, Apartado 7586, Alfragide, 2610-999 Amadora, Portugal

Correspondence: José M.L.M. Palma (jpalma@fe.up.pt)

Abstract. The digital terrain model (DTM), the representation of Earth's surface at regularly spaced intervals, is the first input in the computational modelling of atmospheric ~~flows~~flows. The ability of computational meshes based on high (2 m, airborne laser scanning), medium (10 m, military maps) and low (30 m, shuttle mission, SRTM) resolution DTMs to replicate the Perdigão experiment site was appraised in two ways: by their ability to replicate the two main terrain attributes, elevation and slope, and by their effect on the wind ~~flow~~ flow computational results. The effect on the ~~flow~~ flow modelling was evaluated by comparing the wind speed, wind direction and turbulent kinetic energy by VENTOS®/2 at three locations, representative of the wind ~~flow~~ flow in the region. It was found that the SRTM was not an accurate representation of the Perdigão site. A 40 m mesh based on the highest resolution data, yielded at five reference points an elevation error of less than 1.4 m and an RMSE of less than 2.5 m, compared to 5.0 m, in the case of military maps and 7.6 m in the case of SRTM. Mesh refinement beyond 40 m yielded no or insignificant changes on the ~~flow~~ flow field variables, wind speed, wind direction and turbulent kinetic energy. At least 40 m horizontal resolution–*threshold resolution*–, and based on topography available from aerial survey, is recommended in computational modelling of the ~~flow~~ flow over Perdigão.

1 Introduction

A Digital Terrain or Elevation Model (DTM or DEM) is a representation of the Earth's surface elevation at regularly spaced horizontal intervals. Although the terrain model is the first input in computational modelling of atmospheric ~~flows~~flows, its impact on ~~flow~~ flow results has not been a matter of concern, because the spatial resolution of publicly available DTMs is higher than the size of the computational grid often used to resolve the terrain. However, before a ~~fluid flow~~ fluid flow database (Mann et al., 2017) can be used as a reference in ~~flow~~ flow model appraisal and development, the impact of the terrain modelling must be assessed. For studies of the atmospheric ~~flow~~ flow over Perdigão the publicly available DTMs were considered not accurate enough (Mukherjee et al., 2013; Simpson et al., 2015) and an airborne laser scanning campaign of the region was carried out in 2015~~,~~; first to assist the design of the Perdigão campaigns in 2015 and 2017 (cf., Vasiljević et al., 2017; Fernando et al., 2019) and second, to provide the high resolution terrain data for computational ~~flow~~ flow modelling, on par with the resolution provided by the large number of measuring equipment within a small region.

The Perdigão site is located in the municipality of Vila Velha de Ródão, in the centre of Portugal (608250E, 4396621N: ED50 UTM 29N or in WGS84, 39°42′38.5″N 7°44′18.5″W). It is comprised by two parallel ridges, about 500 m elevation, 4 km length, SE-NW orientation, and distanced around 1.4 km from each other. The land is covered by a mixture of farming areas and patches of eucalyptus (~~*eucalyptus*~~ *Eucalyptus globulus*) and pine trees (~~*pinus*~~ *Pinus pinaster*). The dominant winds are perpendicular to the ridges, assuring a largely two-dimensional ~~flow~~flow.

The accuracy of a DTM depends on the data collection techniques, data sampling density and data post-processing, such as grid resolution and interpolation algorithms. In computational modelling of atmospheric ~~flows~~flows, DTMs are often used from photogrammetry or satellite interferometry, such as *SRTM, Shuttle Radar Topography Mission*, (Farr et al., 2007) or *ASTER, Advanced Spaceborne Thermal Emission and* ~~*Reflection*~~ *Reflection Radiometer* (Yamaguchi et al., 1998), freely available at https://earthexplorer.usgs.gov/. SRTM has the widest cover and is the most commonly used terrain data. Its latest version (V3.0 1", 2014) is 1 arc-second on most of the planet's surface, i.e. about 23.75 m resolution and an absolute height error equal to 6.2 m at Perdigão's latitude (Farr et al., 2007). With the advent of high resolution techniques such as lidar aerial survey, terrain data has become available with resolutions above 10 m and vertical accuracy typically below 0.2 m (Hawker et al., 2018), and the question is whether such high resolution is needed in the computational modelling of atmospheric ~~flows~~ flows over complex terrain.

1.1 Literature review

Grid independent calculations is a concept very dear to computational ~~fluid~~ fluid dynamics practitioners (e.g., Roache, 1998), as a mean for reducing discretisation errors. However, its application in the context of atmospheric ~~flows~~ flows is not that simple, because every level of grid refinement brings another level of surface detail; see for instance the coastline paradox (Mandelbrot, 1967, 1982). In this case, because the ~~flow~~ flow is driven by topography, the ~~flow~~ flow model results are directly correlated to the terrain data and our problem is common to what can be encountered in geomorphology, with applications in hydrology ~~(e.g., Zhang and Montgomery, 1994; Deng et al., 2007)~~(e.g., Zhang and Montgomery, 1994; Wise, 2000; Deng et al., 2007; Savage et al.,

, where the DTM grid size affects the drainage area. In spite of its importance, to our knowledge, there is no systematic study on the appropriate grid size for resolving the terrain in microscale modelling of atmospheric ~~flow~~ flow over complex terrain.

Work has been done in quantifying the impact of using different DTMs and resolution on terrain attributes, such as elevation, slope, plan and profile curvature, and topographic wetness index. For instance, Mahalingam and Olsen (2016) notes that DEMs are often obtained and resampled without considering the ~~influence~~ influence of its source and data collection method. Finer meshes do not necessarily mean higher accuracy in prediction (with examples for landslide mapping where terrain slope has a great ~~influence~~influence) with the DEM source being an important consideration.

DeWitt et al. (2015) ~~compares~~ compared several DEMs (USGS, SRTM, a statewide photogrammetric DEM and ASTER) to a high-accuracy lidar DEM to assess their differences in rugged topography through elevation, basic descriptive statistics and histograms. Root mean square error ~~values found~~ ranged from 3 (using photogrammetric DEM) to circa 15 (using SRTM) or 17 m (using ASTER).

Deng et al. (2007) ~~indicates~~ indicated that the mesh resolution can change not only terrain attributes in specific points but also the topographic meaning of attributes at each point. ~~It concludes~~ They concluded that variation of terrain attributes were consistent with resolution change and that the response patterns were dependent on the landform classes of the area. Deng et al. (2007) ~~introduce~~ introduced the concept of threshold resolution, i.e. the resolution beyond which the model quality deteriorated quickly, but below which no significant improvement in modelling results was observed.

? ~~develops~~ developed an experimental three-step statistical method to determine an adequate resolution in DEM to represent topographic variables and landscape properties at a micro-scale (exemplified by soil moisture) by performing a set of correlation analysis between resolutions.

Diebold et al. (2013) ~~show~~ showed the effect of grid size in LES of ~~flow~~ flow over Bolund. Lange et al. (2017) ~~addresses~~ addressed the question of how to represent the small topographic features of Bolund in wind tunnel modelling, comparing a round and a sharp edge of a cliff in a wind tunnel, to conclude that the ~~flow~~ cliff with the sharp edge gives an annual energy production of a wind turbine near the escarpment that is 20% to 51% of the round-edge case.

1.2 Objectives and outline

The objective of the present study is to determine the terrain resolution required to accurately resolve the atmospheric ~~flow~~ flow over Perdigão and mountainous terrain in general. One needs to assess the terrain horizontal resolution before assessing the effect of other (also important) causes of differences between experimental and computational results. Many computational studies based on Perdigão data are expected and it is important to asses the terrain resolution requirements first.

In what follows, we describe the techniques used for aerial and terrestrial surveying (section 2), plus the post-processing of those data and the determination of the main geometrical parameters of the Perdigão site (section 3). The results on terrain attributes and computational ~~flow~~ flow modelling are the subject of sections 4 and ~~5~~**??**. The paper ends (section 6) with conclusions and recommendations on the most appropriate DTM and grid size required in the computational modelling of the ~~flow~~ flow over Perdigão.

2 Topographical surveying: equipment and techniques

2.1 Airborne laser scanning (2015)

The lidar aerial survey (Mallet and Bretar, 2009) was performed on 15 March 2015 by NIRAS (2015), with assistance from Blom TopEye. The survey covered an area equal to $22\,071\,075\,\mathrm{m}^2$ (Figure 1a) and was completed in one session, at an altitude of 500 m with a TopEye system S/N 444 mounted on a helicopter. The number of points of the lidar point cloud was approximately 993198375, an average point density inside the project area equal to 45 points/m^2.

Lidar data was checked for point density control by Blom's software TPDS (TopEye Point Density and Statistics), with the area being fully covered by lidar data with exceptions for watersheds. ~~Concerning the primary data processing, the GPS data~~ GPS signal was processed using data from three Portuguese reference network stations (CBRA, MELR and PORT, cf. DGT (2017)), ~~switched on 1 sec registration~~ after assistance by the Portuguese National Mapping Agency (*Direção-Geral do Território, Divisão de Geodesia*). Discrepancies between flight lines (based on Blom's software TASQ, TopEye Area Statistics and Qualities, calculated on subareas of 1 m and after matching of 204104275 observation) showed a maximum altitude deviation and RMSE equal to 0.490 m and 0.061 m. In 75% of the subareas the RMSE was lower than $60\,\mathrm{mm}$.

The photography (a total of 851 photos, stored as $300\,\mathrm{m} \times 300\,\mathrm{m}$ GeoTIFF ~~files~~files) was performed with a Phase One iXA180 camera, a medium format, 10328 pixel $\times$ 7760 pixel sensor resolution, yielding a ground resolution equal to $4.7\,\mathrm{cm}$. The delivery comprised orthophotos of $5\,\mathrm{cm}$ and $20\,\mathrm{cm}$ resolution (Figure 1b).

The prodution of the digital terrain model based on the lidar data is the subject of section 3.1.

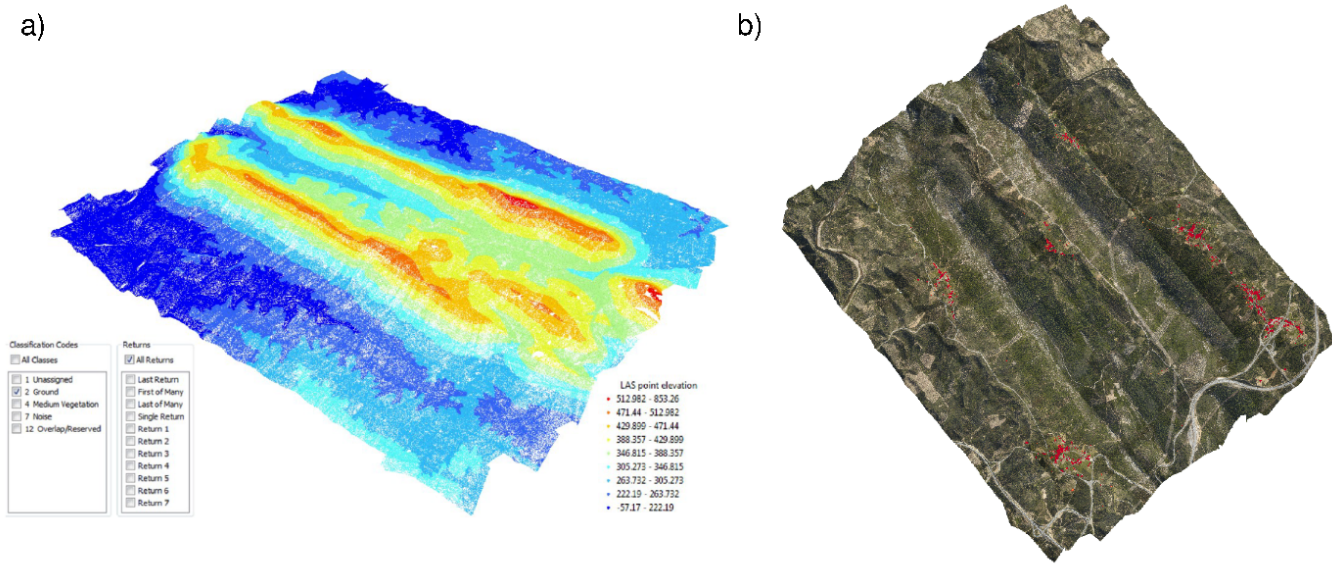

Figure 1. Lidar aerial survey and ortophoto.

2.2 Terrestrial surveying (2017 and 2018)

During the installation of ~~scientific~~ scientific equipment (Nov 2016–May 2017), terrain elevation was measured in situ (Palma et al., 2018) for an accurate and ~~final~~ final determination of the elevation data of part of the instrumentation. The measuring equipment was a Leica system, comprised of the following units: (1) Leica MultiStation MS50, (2) Leica Viva GS14 - GNSS Smart Antenna, (3) Leica CRT16 Bluetooth Cap and (4) Leica GRZ121 360 Reflector PRO Surveying Prism.

In 2017, a piece of land required changes for installation of tower 20/tse04. The topographic survey of that region was carried out (Alves, 2018) and incorporated in the lidar based terrain model as of March 2015. This survey was performed by Spectra Physics (SP60 GNNS receiver and data collector T41 with Survey Pro software) equipment and software by Sierrasoft (PROST Premium/Topko Standart, Version 14.3) for prodution of the local DTM at a 1:500 scale.

3 Terrain model

3.1 Airborne laser scanning (2015)

The lidar data was ~~classified~~ classified in laser pulse classes corresponding to four types of data (ground, vegetation, unassigned and noise) and stored in LASer (LAS) File Format, and then post-processed by tools pertaining to the LAStools© software suite (LAStools, 2019) in three stages, Figure 2.

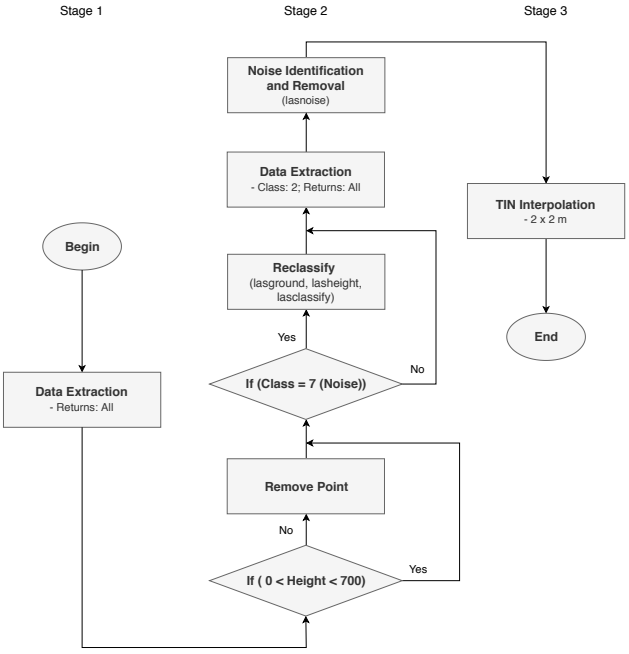

Figure 2. ~~Workflow~~ Workflow diagram for producing the terrain map using LAStools©.

Stage 1 was concerned with the extraction of the lidar raw data. The ground class data were mostly a mesh of regular spaced points, plus a few scattered points and small distinctive areas devoid of points, with abnormal values in their centre, attributed to lidar reading errors.

Stage 2 involved the ~~reclassification~~ reclassification of abnormal data. A ~~first~~ first procedure was used to reclassify a particular area of ~~noise-classified~~ noise-classified points into the ground or vegetation classes, which would otherwise be void of ground points. Points with excessive (>~~700m~~700 m) or negative elevations a.s.l. (above sea level) were removed during this stage. Isolated points above or below the more spatially dense point cloud, ~~classified~~ classified as ground or vegetation, were ~~identified~~ identified and removed using the *lasnoise* tool.

In Stage 3, a Triangulated Irregular Network (TIN), based on the Delaunay triangulation, was obtained for the ground ~~classified~~ classified points. The DTM was obtained by interpolating the heights into a regular mesh with a resolution of 2×2 metre, the highest horizontal resolution of the terrain elevation within the Perdigão site.

3.1.1 Buildings

It is not clear whether a DTM should comprise buildings and other man-made artefacts that are usually part of digital surface models (DSM). In the context of the present study, buildings are long standing structures, as a terrain feature, and we ~~first~~ saw no reason for buildings not being part of the DTM. The houses, in Figure 1b, are family houses of about $15\,\mathrm{m} \times 15\,\mathrm{m}$ and $3\,\mathrm{m}$ height that will show on the ~~finest~~ finest mesh only and as a point elevation. Unless there are a few neighbouring buildings, the ability to resolve isolated houses is limited.

The ~~first~~ first task to include the building data in the DTM, embraced the extraction of unassigned (section 3.1) data points to a point database, containing points representative of obstacles, buildings or other types of structures detected by the lidar and different from vegetation or ground points. The second task involved the digitalization of all buildings from the orthophotos. This process was needed to retain the building polygons as close as possible to their exact shape and exclude possible outliers captured by the automatic points extraction, and also to perform a more effective and precise interpolation of the data. The third and ~~final~~ final stage was the interpolation of the buildings points included inside the digitized polygons for a continuous representation of the buildings. The interpolation scheme used in the ArcGIS platform (ESRI, 2016) was the natural neighbour method (Sibson, 1981), which preserves the shapes boundaries (Watson, 1994).

Calculations including the building data showed minor or no visible ~~flow~~ flow changes and were discarded.

3.2 Two-dimensionality and main geometrical parameters

One of the reasons why Perdigão was selected was its geometry; namely, the parallelism between the two ridges and their large length relatively to the width, bringing the orography close to two-dimensionality.

3.2.1 Area of interest (AOI), reference lines and locations

For scaling and dimensional analysis, the main geometrical parameters of the Perdigão site were determined and the area of interest (AOI) was ~~defined~~ defined (Figure 3 and Table 1): a rectangular shape of aproximately ($3\,\mathrm{km} \times 4\,\mathrm{km}$), with lower left corner at 608589E; 4394131N and aligned with the centreline (ℓ_C, SE-NW direction, 135°). This area, centred near station 131, included the SW and the NE ridge, the valley and the location of most of the instrumentation deployed in Perdigão. Note that the coordinate system was converted from ETRS89 PT-TM06 (original source) to ED50 UTM29 and will be used throughout the document as Eastings and Northings. Stations number (#) and code as in Perdigão web site (perdigao.fe.up.pt/).

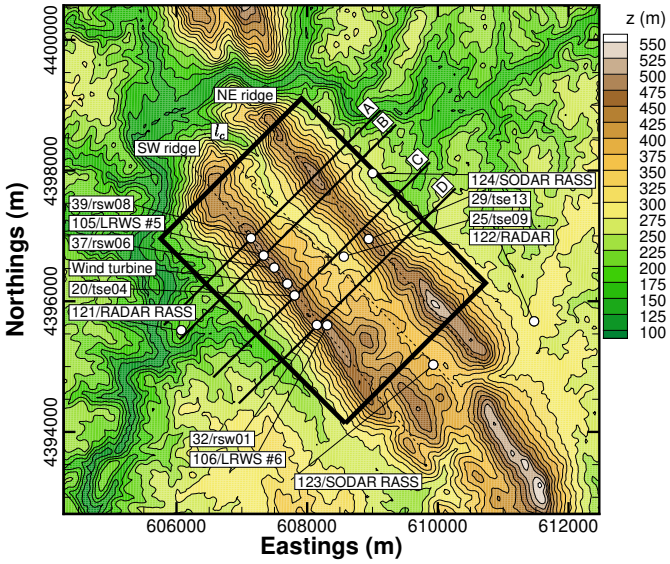

Figure 3. Area of interest and transects (ED50 UTM 29N).

3.2.2 Terrain ~~profile~~ profile and slope

The terrain ~~profile~~ profile (Figure 4) is not uniform along the valley, which becomes narrower and deeper along the SE-NW direction. For instance, the NW ridge height relative to a reference height (h_{ref}, the mean height of the surrounding terrain in a $20\times20\,\mathrm{km}$ area) equal to 250 m a.s.l. varies between ~~201.06 and 251.36~~201.1 and 251.4 m, and the distance between ridges is ~~1358.00 and 1480.00 m~~ 1358. and 1480.0 m on transects A and D (Table 2).

Apart from ℓ_C, six additional lines were ~~defined~~defined: ℓ_{SW} and ℓ_{NE} along the SW and the NE ridges, and A, B, C and D, perpendicular to the ridges (SW-NE direction, 225°) and related to four main transects: A and D that delimit the northernmost (station 39) and southernmost (station 32) locations of the great majority of the instrumentation; and transects B and C that delimit a narrower region, determined by locations of stations 105/LRWS#5 and 20/tse04.

Table 1. Reference points as in Figure 3 (ED50 UTM 29N).

#	Type/Code	Eastings (m)	Northings (m)	Elevation (m)
	Wind turbine	~~607697.43~~ 607697.	~~4396268.40~~ 4396268.	484.0
20	20/tse04	~~607808.15~~ 607808.	~~4396089.94~~ 4396090.	473.0
25	25/tse09	~~608561.10~~ 608561.	~~4396683.01~~ 4396683.	305.3
29	29/rsw01	~~608938.98~~ 608939.	~~4396953.43~~ 4396953.	452.9
32	32/rsw01	~~608148.76~~ 608149.	~~4395637.77~~ 4395638.	472.1
37	37/rsw06	~~607497.90~~ 607498.	~~4396514.05~~ 4396514.	482.5
39	39/rsw08	~~607140.01~~ 607140.	~~4396966.32~~ 4396966.	488.9
105	LRWS #5	~~607334.63~~ 607335.	~~4396700.65~~ 4396701.	485.9
106	LRWS #6	~~608306.93~~ 608307.	~~4395634.00~~ 4395634.	486.3
121	RADAR/RASS	~~606073.73~~ 606074.	~~4395557.68~~ 4395558.	223.7
122	RADAR	~~611473.79~~ 611474.	~~4395693.69~~ 4395697.	288.6
123	SODAR/RASS	~~609930.76~~ 609931.	~~4395029.08~~ 4395029.	361.9
124	SODAR/RASS	~~609002.59~~ 609003.	~~4397960.14~~ 4397960.	258.4

Other geometric variables (Figure 4) are the height of ridges (h_{SW} and h_{NE}) and valley (h_{val}) relative to the reference height (h_{ref}), the half-widths of the ridges ($l_{SWw}, l_{SWe}, l_{NEw}$ and l_{NEe}) at half-height ($h_{SW}/2$ and $h_{NE}/2$), and the distance between ridges, ℓ.

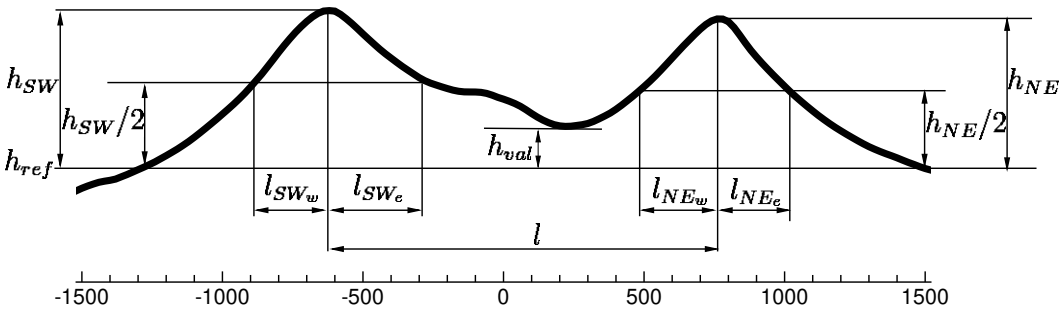

Figure 4. Terrain profile: geometrical parameters.

The ridges' orientation was determined by a linear regression of two z maxima, for each j (mesh oriented with SW-NE direction) on a $20\,\mathrm{m}$ grid, between transects A and D ($\approx 1650\,\mathrm{m}$) and between transects B and C ($\approx 530\,\mathrm{m}$). The deviations from parallelism are $4.3°$ if restricted to the region between A and D. Between transects B and C, where the core of the instrumentation was, the ridges were parallel within $2.8°$; i.e., $139.1°$ and $136.3°$ in the case of SW and NE ridges. The slope

Table 2. Main geometric variables of transects A, B, C and D (slope (S) in degrees (°), and length and elevation (ℓ and h) in metre, $h_{ref} = 250$ m a.s.l.).

	A	B	C	D	Average
h_{SW}	~~237.22~~ 237.2	~~237.32~~ 237.3	~~228.26~~ 228.3	~~221.96~~ 222.0	~~231.19~~ 231.2
h_{NE}	~~251.36~~ 251.4	~~212.65~~ 212.7	~~205.29~~ 205.3	~~201.06~~ 201.1	~~217.59~~ 217.6
h_{val}	~~24.52~~ 24.5	~~31.14~~ 31.1	~~46.79~~ 46.8	~~65.23~~ 65.2	~~41.92~~ 41.9
l_{SWw}	~~277.81~~ 277.8	~~214.03~~ 214.0	~~232.04~~ 232.0	~~212.26~~ 212.3	~~234.04~~234.0
l_{SWe}	~~269.96~~ 270.0	~~304.99~~ 305.0	~~402.87~~ 402.9	~~432.00~~ 432.0	~~352.46~~352.5
l_{NEw}	~~286.87~~ 286.9	~~320.16~~ 320.2	~~249.47~~ 249.5	~~268.69~~ 268.7	~~281.30~~281.3
l_{NEe}	~~258.35~~ 258.4	~~244.94~~ 245.0	~~221.91~~ 221.9	~~261.74~~ 261.7	~~246.74~~246.7
l	~~1358.00~~ 1358.0	~~1384.00~~ 1384.0	~~1412.00~~ 1412.0	~~1480.00~~1480.0	~~1408.50~~1408.5
S_{SWw}	~~33.64~~ 33.6	~~37.47~~ 37.5	~~36.78~~ 36.8	~~39.99~~ 40.0	~~36.97~~ 37.0
S_{SWe}	~~-45.09~~ -45.1	~~-29.60~~ -29.6	~~-22.68~~ -22.7	~~-21.08~~ -21.1	~~-29.61~~-29.6
S_{NEw}	~~30.65~~ 30.7	~~25.69~~ 25.7	~~27.81~~ 27.8	~~25.69~~ 25.7	~~27.46~~ 27.5
S_{NEe}	~~-35.74~~ -35.7	~~-30.05~~ -30.1	~~-30.65~~ -30.7	~~-24.11~~ -24.1	~~-30.14~~-30.1

($S = |\text{atan}(h_{SW,NE}/2)|/\ell_{SW,NE}$), also on a 20 m grid varies between 21.08° and 45.09°, always above the threshold for ~~flow separation~~ flow separation under neutral conditions (Wood, 1995).

4 Digital terrain model: results and discussion

The terrain elevation and slope are the two main terrain attributes for ~~classification~~ classification of terrain complexity and the ones to replicate accurately by terrain models. In this section, three DTMs of the Perdigão site are analysed within the AOI, by comparing terrain elevation and slope on meshes based on these terrain models with the terrain elevation and slope measured by the lidar aerial survey data within the AOI.

The three DTMs (Figure 5 and section 4.4) were the following: (1) ALS, the area sampled by lidar with a 2 m resolution (~~file~~ file #1 of Topography data on page 24); (2) Military, the Portuguese Army cartography around Perdigão, 10 m horizontal resolution (~~file~~ file #2 of Topography data on page 24) available from Portuguese Army Geospatial Information Centre (*CIGeoE Centro de Informação Geoespacial do Exército*), a total of eight sheets (numbers 290.4, 291.3, 302.2, 302.4, 303.1, 303.3, 313.2 and 314.1) at a scale equal to 1:25000; and (3) SRTM, the SRTM 30 m (~~file~~ file #3 of Topography data on page 24).

Because the ALS was the highest resolution map, and the most accurate representation of the terrain in Perdigão, it was the one against which the accuracy of alternative terrain data sources was evaluated.

Concerning the terrestrial surveys in 2017 and 2018 (section 2.2), a sample of those measurements ~~confirmed~~ confirmed the high quality of lidar airbone measurements. The survey carried in 2018, showed that the terrain change due to installation of tower 20, yielded alteration of the terrain that were not ~~significant~~ significant (lower than 1 m).

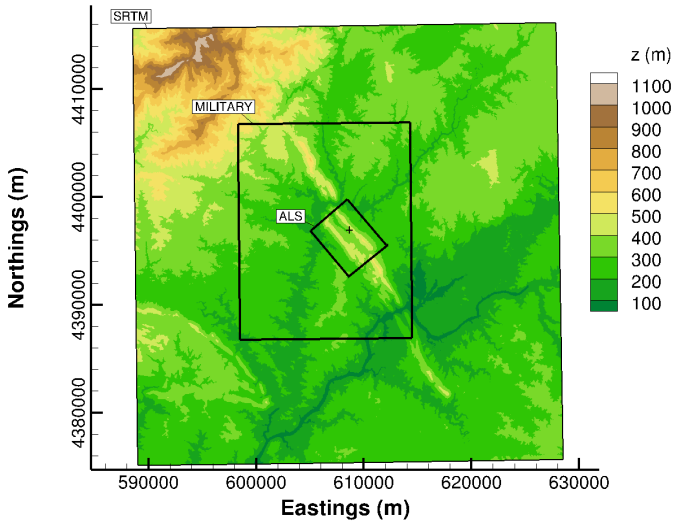

Figure 5. Total area comprised by SRTM, military and airborne data (+: domain centre).

4.1 Mesh generation

For comparison of terrain attributes, elevation and slope, regularly spaced meshes of 80, 40, 20 and 10 m (size, $n_i \times nj$, respectively 39×51, 77×101, 153×201 and 305×401) were generated within the AOI. The resampling procedure was similar to Deng et al. (2007); i.e., one out of two points was retained to assure that every point in the coarser resolutions existed on the ~~finer~~ finer ones. Coarser meshes are resampled versions of the 2 m resolution mesh, obtained by removing additional nodes.

4.2 Elevation at ~~five~~ five reference points

Five points (Table 1) were selected for DTM comparison: towers 20/tse04, 25/tse09 and 29/tse13, the three 100 m meteorological towers, comprising a transect aligned with the dominant wind direction, and tower 37/rsw06 and the wind turbine location, along the SW ridge.

Figure 6 shows the absolute error ($z_{error} = z_{80,40,20,10} - z_2$), difference between the elevation at a given mesh and DTM source, with respect to the terrain elevation on the reference mesh (ALS_2). In the case of SRTM based meshes (Figure 6a), the error tends to a plateau at resolutions equal to 40 m. Similar behaviour is found in the case of the Mil database (Figure 6b), but at 20 m resolution; 20 and 10 m mesh increases the error at 20/tse04 and meshes at higher resolution to the uncertainty of this database must be avoided. Contrary to the SRTM and Mil, when using ALS (Figure 6c), with mesh ~~refinement~~ refinement there is a noticeable error reduction at all 5 points.

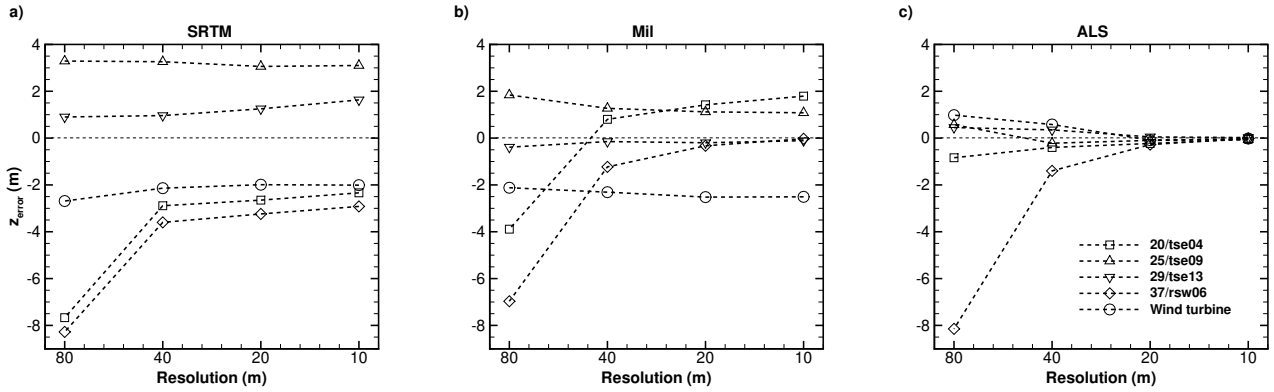

Figure 6. Impact of mesh resolution on reference points: a) SRTM; b) Mil; c) ALS.

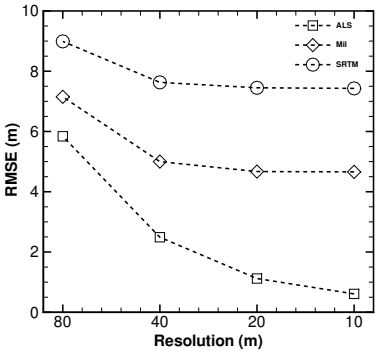

Figure 7. Impact of mesh resolution on RMSE.

4.3 Elevation and slope in the area of interest (AOI)

As the DTM quality increased from SRTM to Mil and ALS, the maximum terrain elevation (z_{Max}) also increased, from 530.2 to 540.5 and 540.8 m, and the minimum (z_{Min}) decreased from 165.0 to 158.8 and ~~150.7~~156.8 m (Table 3). Maxima and minima terrain elevations are set by the DTM source; maxima and minima are similar for a given DTM regardless of the grid size, which was a consequence of the procedure for mesh ~~refinement.~~ refinement. The 10 m difference between SRTM and the ALS values is consistent with the RMSE of SRTM, equal to 6.2 m for Eurasia (Table 1, Farr et al., 2007) and also with the conclusions by DeWitt et al. (2015).

The error distribution (Figures 8 and 10a) shows an overprediction of the terrain elevation along the valley and an underprediction along the ridges, with both much reduced between the 80 and the 40 m resolution meshes, with the latter showing a mostly uniform error distribution of around 1 m (Figure 8b).

Table 3. Maxima and minima terrain elevation, based on SRTM, Mil and ALS data.

	z_{Max} (m)			z_{Min} (m)		
Mesh	SRTM	Mil	ALS	SRTM	Mil	ALS
80	530.2	538.4	537.3	165.0	159.4	~~146.0~~157.0
40	530.2	538.4	537.9	165.0	159.4	~~149.2~~157.0
20	531.1	540.0	~~539,4~~ 539.4	165.0	158.8	~~150.3~~156.8
10	531.4	540.5	540.8	165.0	158.8	~~150.7~~156.8
2	-	-	541.1	-	-	~~155.2~~156.8

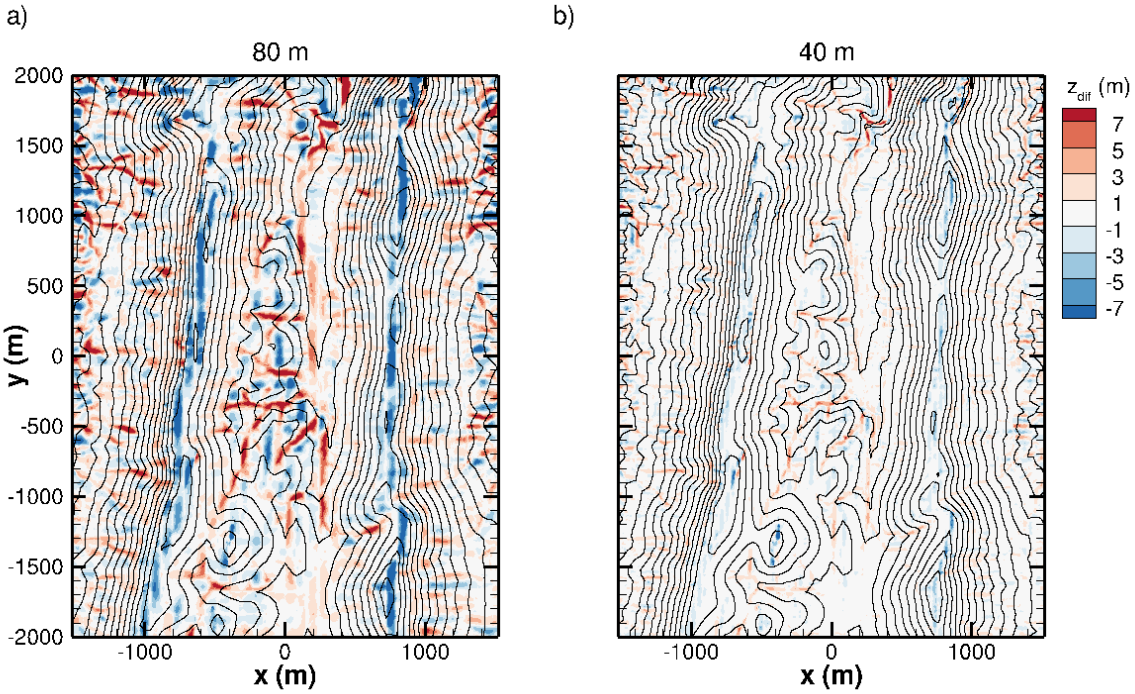

Figure 8. Elevation error of resampled meshes (ALS terrain data) over the AOI surface: a) 80 m mesh; b) 40 m mesh

.

The RMSE error (Figure 7) over the whole AOI is consistent with the elevation error and the inherent uncertainty of every DTM source; with mesh ~~refinement~~ refinement every DTM tends to its resolution level. The minimum RMSE of SRTM, Mil and ALS are 7.43, 4.66 and 0.61 m at resolutions of 10 m.

The maximum slope (55.85° and 64.76°) was about 50% higher on 20 and 10 m meshes compared with the coarser resolution (37.31° and 44.24° meshes, 80 and 40 m), Table 4. The negative slope increased from $-37.33°$ to $-67.81°$, as the resolution increased from 80 to 10 m. The histogram of the slope in the x (SW-NE, 225°) direction (Silva, 2018) shifted to the right, as

Table 4. Maxima and minima slope in the x (SW-NE, 225°) direction, based on SRTM, Mil and ALS terrain data.

	S_{Max} (°)			S_{Min} (°)		
Mesh	SRTM	Mil	ALS	SRTM	Mil	ALS
80	39.00	38.27	37.31	-36.11	-37.99	-37.33
40	41.61	43.10	44.24	-38.64	-47.61	-51.74
20	44.65	49.36	55.85	-47.18	-55.19	-59.31
10	47.86	51.74	64.76	-49.02	-61.31	-67.81
2	-	-	75.91	-	-	-81.13

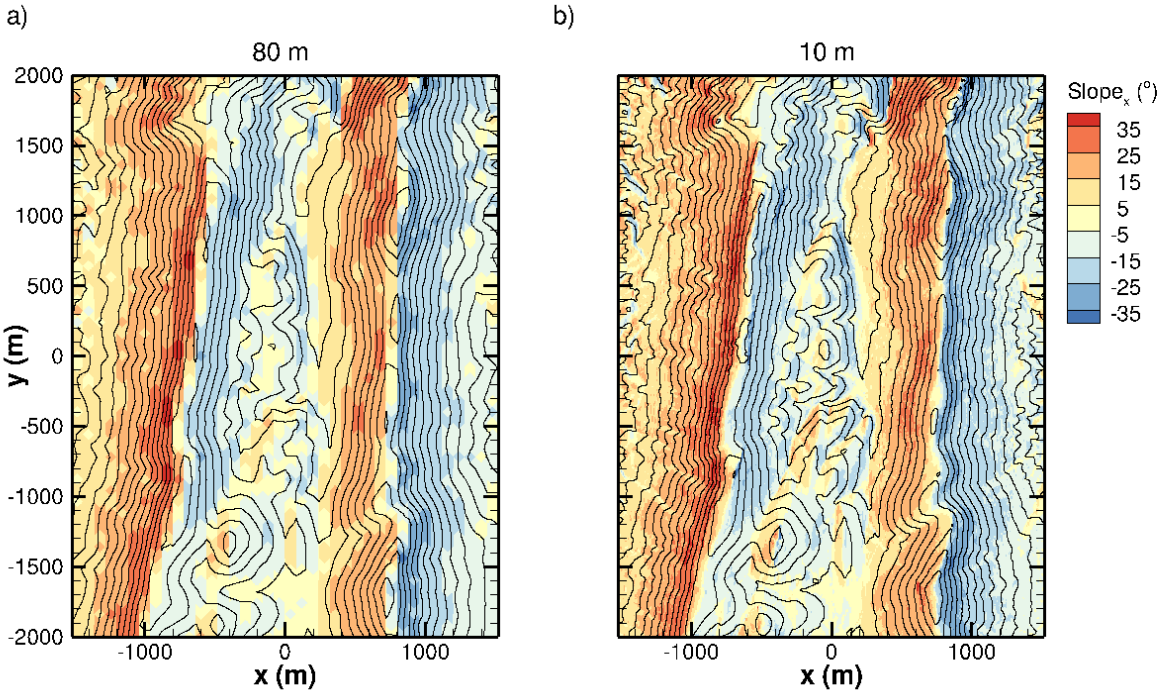

Figure 9. Slope in x (SW-NE, 225°) direction with different resolutions mapped on AOI's surface (ALS terrain data): a) 80 m mesh; b) 10 m mesh

.

the content at low slopes, decreases and more and more higher slope locations were resolved. Because the ridges are quasi two-dimensional, the y (SE-NW, 135°) direction slope was residual (Silva, 2018) compared to the x direction slope (Figure 9) and is not shown here.

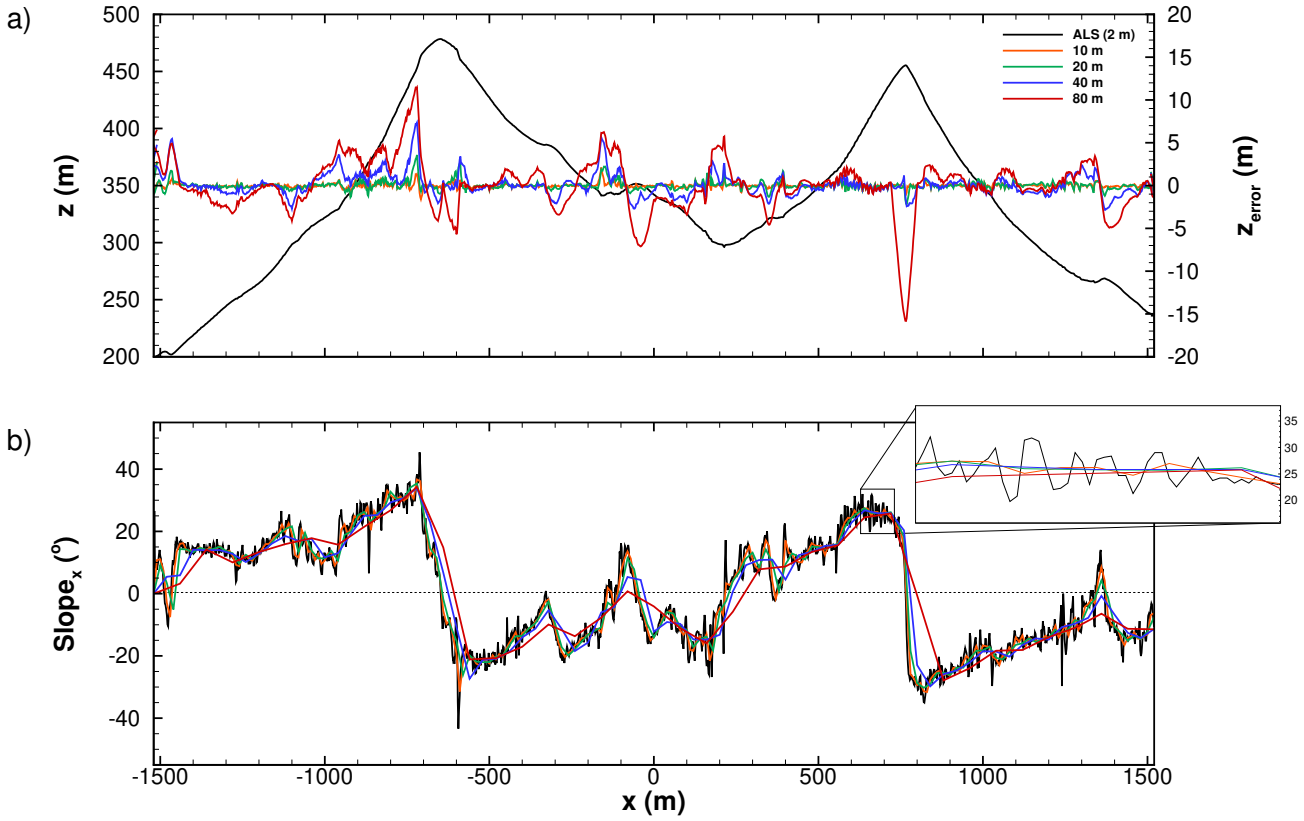

Figure 10. Elevation and slope in the x direction ~~profiles~~ profiles on a plane that contains tower 20/tse04 (ALS terrain data).

The larger errors occurred at locations of higher slope (Figure 10) and these are the locations where the grid ~~refinement~~ refinement was also the most effective in reducing the elevation error. For instance, errors equal to $11.5\,\mathrm{m}$ and $-15.8\,\mathrm{m}$ (at $x = -720\,\mathrm{m}$ and $x = 766\,\mathrm{m}$) on a 80 m mesh were reduced to $7.5\,\mathrm{m}$ and $-2.5\,\mathrm{m}$ on a 40 m mesh.

4.4 Spectra analysis

Spectra of terrain elevation show the ALS resolution one order of magnitude higher compared to SRTM data (Figure 11). The ~~figure~~ figure also displays two scaling ranges, typical of global topographies (e.g., Nikora and Goring, 2004), with exponents equal to -7/4 and - 11/3.

As expected, there is an increase in resolved spectral range with mesh ~~refinement~~ refinement and an overlap between meshes with ALS data. In the case of SRTM and Mil based meshes, linear ~~refinements~~ refinements (20 and 10 m meshes) cannot replicate the decay for higher frequencies and overcome the inherent resolution of the original data. Mesh quality was as good as the terrain data source. Only meshes based on the ALS have the ability to reproduce accurately the high-frequency range

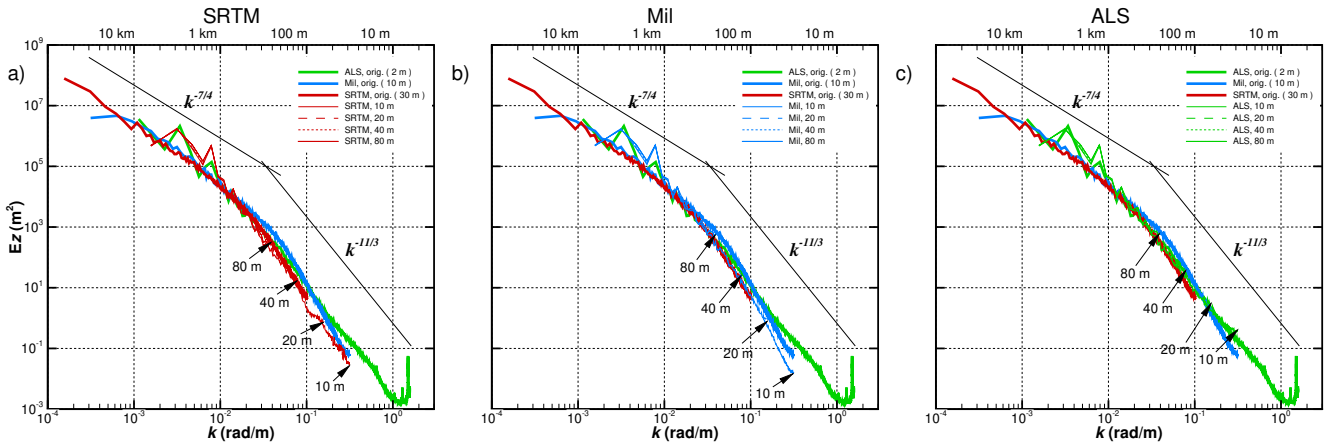

Figure 11. Spectra analysis for DTM and meshes.

225 ($10^{-1}\,\mathrm{rad\,m^{-1}} < k < 1\,\mathrm{rad\,m^{-1}}$). SRTM is restricted to around 30 m resolution and meshes 20×20 and 10×10, with identical z_{Max} and z_{Min} (531 and 165 m), are unable to replicate the ALS measured values, z_{Max} and z_{Min}, Table 3. Grid ~~refinement~~ refinement cannot go beyond the inherent resolution of the DTM.

4.5 RIX (ruggedness index)

The RIX (ruggedness index) is one of the major parameters in WAsP (Mortensen et al., 2004). It has the goal of quantifying the
230 terrain complexity. The operational envelope of WAsP corresponds to a RIX value of 0%. The ALS data shows a maximum of 23.7% and an overall higher value of RIX (average 15.22%), while SRTM reaches 19.7% (average 11.06%). Lower resolution terrain data underestimate the terrain complexity.

5 Flow modelling

In this section, the results of computational runs on different meshes are discussed. A set of experimental data (UCAR/NCAR-EOL, 2019)
235 (30 minutes averaged) on 4 May 2017, 22:09–22:39 UTM is also included~~, for guidance only; because computational results do not consider, for instance, surface cover heterogeneity or stratification, discrepancies are expected when compared with experimental data~~. This was the day and the time when the assumption of conditions of ~~both stationarity and neutral flow in Perdigão could be made, according respectively with Carvalho (2019)and Palma et al. (2019), and therefore approach the steady-state regime and neutral atmospheric conditions of the computational runs.~~ stationarity based on measurements at tower
240 20/tse04 were valid, according with Carvalho (2019), and the flow was non-stratified based on a bulk Richardson number (R_B) equal to -0.03

$$R_B = \frac{g\left(\overline{\theta}_{100} - \overline{\theta}_2\right)\Delta z}{\overline{\theta}_{100}\left[(U_{100})^2 + (V_{100})^2\right]} \tag{1}$$

where $\overline{\theta}_{100}$ and $\overline{\theta}_2$ are the mean potential temperature at 100 m and 2 m a.g.l (above the ground level), $\Delta z = 100$ m, and U_{100} and V_{100} are the mean horizontal components of the velocity vector also at 100 m a.g.l. . The temperature obtained from measurement data was converted into potential temperature using the following approximation (Stull, 1988):

$$\overline{\theta} \approx \overline{T} + \left(\frac{g}{c_p}\right) z \tag{2}$$

The data set choice was conditioned by the computational flow model being used. Because computational results do not consider, for instance, surface cover heterogeneity, discrepancies are expected when compared with experimental data, which are included here for guidance only.

5.1 Computational ~~flow~~ flow model

The computational code VENTOS®/2 ~~(cf., ?Palma et al., 2008)~~(cf., Castro et al., 2003; Palma et al., 2008), developed for atmospheric ~~flows~~ flows over complex terrain, was used in steady state formulation. It solves the ~~RaNS~~ Reynolds-averaged Navier Stokes set of equations for a turbulent ~~flow ($\kappa - \varepsilon$~~ flow ($k - \varepsilon$ model), with a terrain-following structured mesh, allowing also the simulation of forested terrain ~~and wind turbines~~(Lopes da Costa et al., 2006) and wind turbine wakes (Gomes et al., 2014; Gomes a .

5.1.1 Integration domain and boundary conditions

The model topography (domain size, $19\,\mathrm{km} \times 18.8\,\mathrm{km}$, around the central location 608250E, 4396621N) was obtained by bi-linear interpolation of terrain data. The positioning of the domain boundaries and its impact on ~~flow~~ flow variables were part of the work of Silva (2018).

At the inlet a log-law ~~profile~~ profile was set. To ensure an equilibrium shear stress, the k ~~profile~~ profile decreases with the square of height above ground level. At the top of the domain a zero shear stress condition was used. The inlet ~~profile~~profile's development is caped at the boundary layer's limit, all quantities being constant above that height. At the lateral boundaries a symmetry condition was applied.

The ground was modelled as a rough surface, a wall function, a log-law ~~defining~~ defining the velocity at the node closest to the ground, and the turbulence model quantities, k and ε. The values used in the computational model for z_0 (roughness length) and u_* (friction velocity) were 0.1 (indicated by Wagner et al. (2019) as the roughness length near the double ridge area after conversion from the CORINE Land Cover classes) and 0.25. These values were uniform for the whole domain. The surface cover (forest patches and height) and its representation in the computational model (roughness length, leaf area index, use of a canopy model) is still a work in progress, as the presence of eucalyptus and pine tree patches in the area are expected to have a decisive impact on the ~~flow~~flow.

5.2 Computational meshes

A total of 18 computational meshes (Table 5) was used. The central part of the domain ($4\,\mathrm{km} \times 6\,\mathrm{km}$, based on ALS and Mil terrain data), was resolved with uniform horizontal resolution ($20 \times 20, 40 \times 40$ and 80×80 m), expanding towards the domain boundaries with factors f_x and f_y close to 1, to minimise the discretisation errors. The domain's height (3000 m) was discretised by 100 nodes (n_k), with the ~~first~~ first node 2 m above ground level and a grid expansion $f_z = 1.0435$, yielding a maximum cell size (Δ_z) equal to 124 m.

A preliminary analysis showed that the ~~flow~~ flow variables had low sensitivity to the number of nodes in the vertical (n_k), opposed to the height of the ~~first~~ first node above ground level, which showed a ~~significant~~ significant impact and is worthy of further studies.

Three types of meshes were used: SRTM, with the whole domain based on the SRTM data; Mil, a combination of SRTM and Military maps; and ALS, based on all three DTM sources (Figure 5). A minimum of 8818 iterations and 3.87 hours of computing time were required, and a maximum of 20033 iterations and $50\times$ more computing time in the case of mesh Mil.NE.20. Number of iteration is a better indicator of the actual computing time, since the value given here was ~~influenced~~ influenced by the computer load at the time of the calculations.

5.3 Flow pattern

The ~~flow~~ flow modelling analysis was based on the ~~flow~~ flow patterns at two transects in the case of SW and NE winds (Figures 12 and 13) and wind speed, wind direction and turbulent kinetic energy results for SW (Figures 14–16).

As expected, the ~~flow~~ flow pattern (Figures 12 and 13) is characterised by separated ~~flow~~ flow regions in the leeside of either ridges. The ~~figures~~ figures are coloured by the spanwise velocity component (v), showing two different streams: up-valley on the leeside of SW ridge and down-valley on the upwind side of NE ridge (Figure 12) and down-valley in the case of NE winds (Figure 13).

The ridge height increases with the grid resolution (see insets) and the detachment point ~~also~~ moves to higher elevations, yielding longer and deeper separated ~~flow~~ flow regions, see for instance Figure 13. ~~In the case of SW winds (Figure 12) the 20 and~~ Menke et al. (2019), in their analysis of the experimental data, reported average length and depth equal to 697 and 157 m for both SW and NE wind directions and stratification levels based on the gradient Richardson number between -1 and 1; in the case of neutral flow, length and height equal to 807 and 192 m were reported for a 10-min period. The length and height of the separation zone, in Table **??**, tend to increase with the grid refinement (with the exception of the SW winds when refining from 40 to 20 m resolution~~meshes yield similar results and appear to be accurate enough for computational modelling of atmospheric flow over Perdigão.~~), predicting a recirculation region longer and narrower compared with the measurements.

5.4 Southwesterly winds

The wind speed, wind direction and turbulent kinetic energy ~~profiles~~ profiles at towers 20/tse04, 25/tse09 and 29/tse13 (Figures 14, 15 and 16) show ~~that in general, there was a poor agreement~~ a good agreement of the wind direction with the

Table 5. Computational meshes ($\Delta z_{Min} = 2\,\mathrm{m}$).

	Name	$\Delta_{x/y}$ min (m)	$\Delta_{x/y}$ Max (m)	$n_i \times n_j$	t_{CPU} (h)	N_{iter}
1	SRTM.SW.80	80	478.6	120×155	6.27	8818
2	SRTM.SW.40	40	400.0	200×270	52.96	11557
3	SRTM.SW.20*	20	414.0	320×470	-	-
4	Mil.SW.80	80	478.6	120×155	18.13	8906
5	Mil.SW.40	40	400.0	200×270	89.64	11040
6	Mil.SW.20	20	414.0	320×470	237.35	14095
7	ALS.SW.80	80	478.6	120×155	3.87	8898
8	ALS.SW.40	40	400.0	200×270	15.09	10996
9	ALS.SW.20	20	414.0	320×470	111.28	16606
10	SRTM.NE.80	80	478.6	120×155	19.92	9554
11	SRTM.NE.40	40	400.0	200×270	110.04	14227
12	SRTM.NE.20	20	414.0	320×470	242.57	15188
13	Mil.NE.80	80	478.6	120×155	28.43	9313
14	Mil.NE.40	40	400.0	200×270	101.90	13351
15	Mil.NE.20	20	414.0	320×470	191.38	20033
16	ALS.NE.80	80	478.6	120×155	3.74	9322
17	ALS.NE.40	40	400.0	200×270	93.49	11937
18	ALS.NE.20	20	414.0	320×470	80.21	18634

	Expansion factors		
min($\Delta_{x/y}$)	f_x	f_y	f_z
80	1.0524	1.0331	1.0435
40	1.0471	1.0299	1.0435
20	1.0518	1.0271	1.0435

* Did not meet residual criteria

measurements~~: wind speed underprediction~~ , a poor agreement of the wind speed (underprediction) at all towers, ~~whereas~~ and underprediction of the turbulent kinetic energy ~~was overpredicted at the top of the SW ridge (20/tse04, Figure 14c) and underpredicted~~ in the valley and at the NE ridge (towers 25/tse09 and 29/tse13, Figures 15c and 16c). A good agreement between computational and experimental results is not expected, mainly because of the uniform roughness length; the important is the sensitivity of the computational results to the different numerical meshes.

~~Lower wind speed at tower 20/tse04 (Figure 14a) is an indication that the inlet conditions and wall parameters (z_0 and u_*) were too high, yielding a high loss of momentum along the 10000 m upstream of this tower. Computational results showed a~~

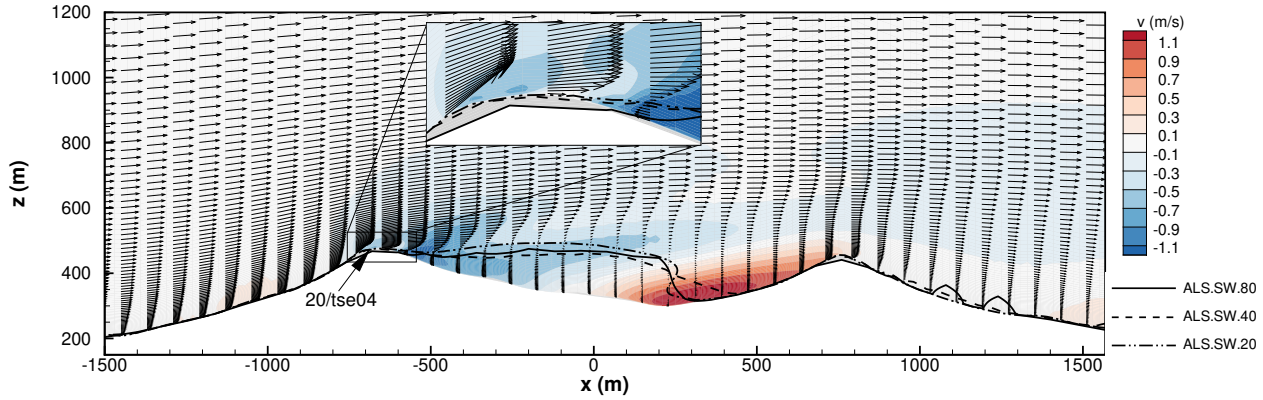

Figure 12. Impact of mesh resolution on separation zone in transect that crosses Tower 20/tse04, in the case of SW winds.

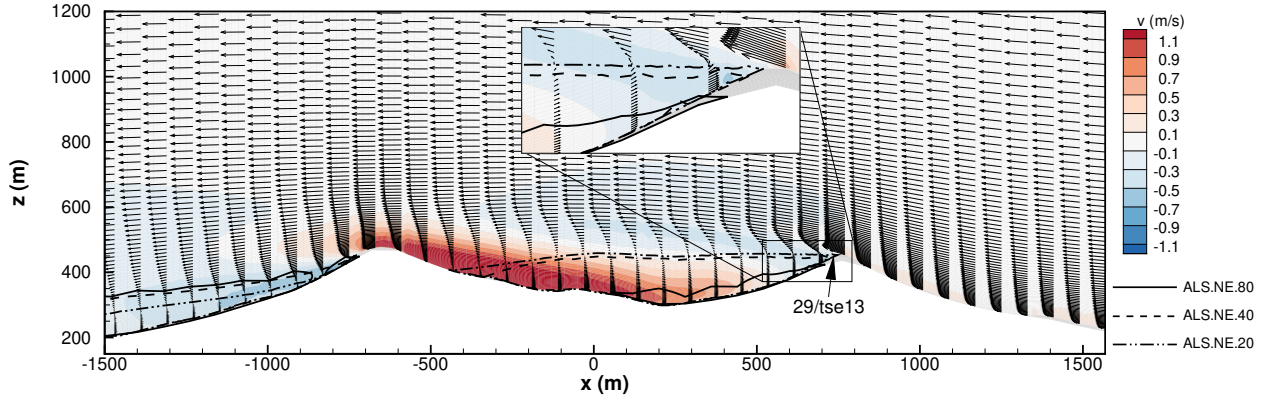

Figure 13. Impact of mesh resolution on separation zone in transect that crosses Tower 29/tse13, in the case of NE winds.

good approximation to wind direction profiles for the three towers, little or no flow deviation was found between the inlet, the top of the southern ridge (As an indicator of stationarity, the mean values of the experimental results over the 30-min period are plotted such as the minima and maxima within that period. Departure from stationarity condition reaches a higher magnitude in the valley (Figure 15), given the location of tower 2025/tse04)and the top of the northern ridge (tower 29/tse04).

Tower tse09 inside the recirculation zone. Unsteadiness is a well-known characteristic of recirculation zones and their prediction is very sensitive to spatial resolution (Castro et al., 2003) and terrain model as shown by Figure 15b. The separated flow region, tower 25/tse09 (Figure 15a) is inside the separated flow region, which explains the) is characterised by low wind speed . This separated flow region is characterised by a and rotation of the wind with the distance above the ground. The flow wind speeds at $z_{asl} > 100$ decreases as the mesh is refined and the height of the recirculation zone increases (Table **??**). The

Table 6. ~~Impact~~ Length and maximum depth of ~~mesh resolution on~~ separation zone~~in transect that crosses Tower 20/tse04~~.

~~Impact of mesh resolution on separation zone in transect that crosses Tower 29/tse13.~~

	Length (m)	Height (m)
Southwesterly winds		
80	1040.1	142.9
40	1120.0	131.8
20	1000.1	155.0
Northeasterly winds		
80	762.5	135.1
40	1120.9	143.4
20	1159.3	151.8

flow in the valley is aligned with the valley and therefore perpendicular to the ridges and the incoming wind. ~~For some reason, in the valley the best~~ The predicted wind direction is in close agreement with the ~~experimental data occurred in the case of the coarser meshes~~ measurements, with the exception of 40 and 20 m meshes based on Mil DTM.

As a whole, ~~results depend more on~~ the flow results appear to be more sensitive to the resolution than ~~on the DTMand at~~ to the DTM; see, for instance, Figure 14a) with the results on 40 and 20 m meshes detached from results on the 80 m mesh. At least a resolution of 40 m is required. ~~Differences between the computational results on 20 and 40 m resolution meshes are minor and within the uncertainty of computational modelling.~~

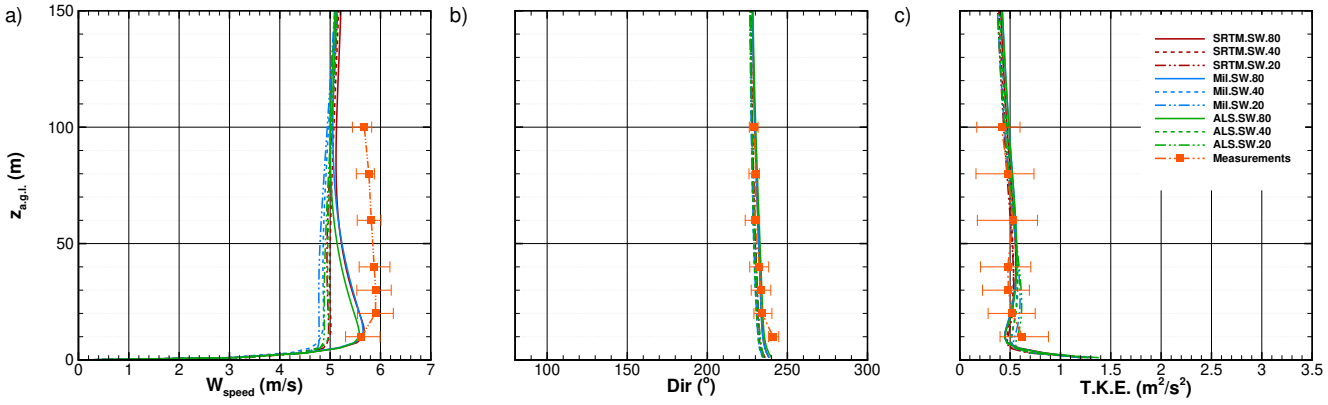

Figure 14. Wind speed, direction and turbulent kinetic energy profile simulation results in tower 20/tse04 for SW winds.

The ~~profiles~~ profiles (not shown) in the case of NE winds (45°) are similar to SW winds, apart from the situation being reversed, since in this case the ~~first~~ first and second ridge are the NE and SW ridges.

Differences between the ~~profiles~~ profiles and the reference ~~profile~~ profile ALS_{20} were measured in terms of RMSE (Tables 6, 7 and 8)~~where~~ , which, in general, show a pattern similar to the slope (Table 4)~~can be observed.~~ , where the RMSE decreases either by refining the mesh or for a given mesh by moving from the SRTM, to Mil and ALS based meshes. RMSE values at

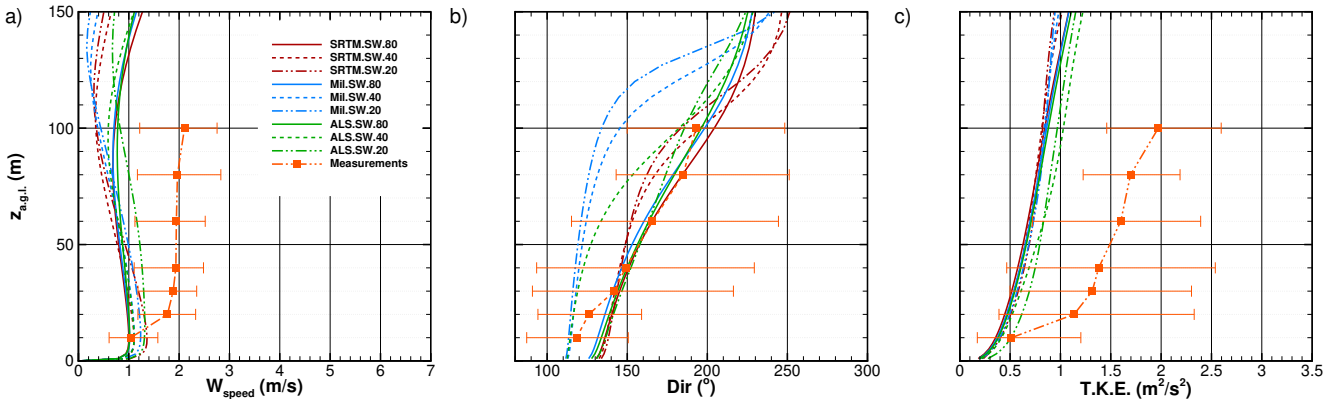

Figure 15. Wind speed, direction and turbulent kinetic energy ~~profile~~ profile simulation results in tower 25/tse09 for SW winds.

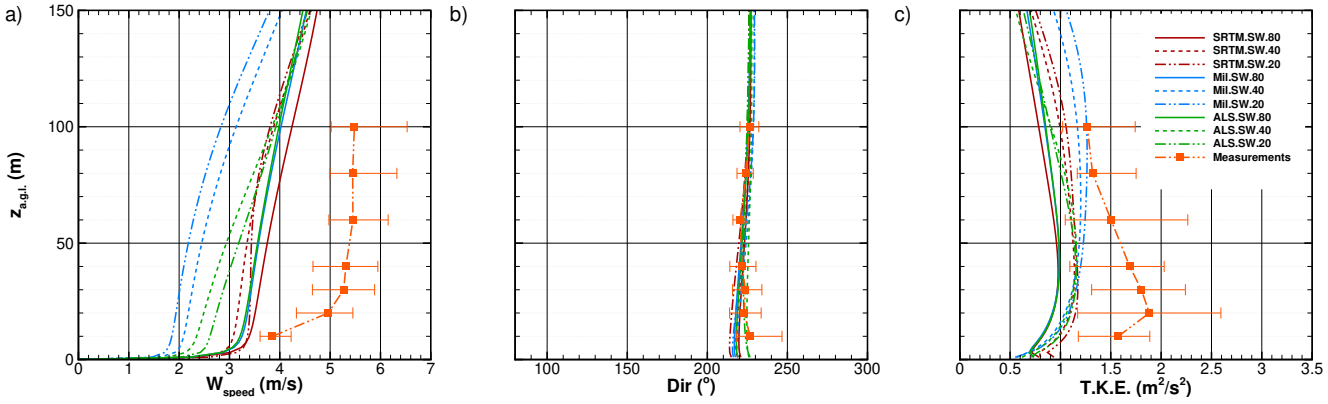

Figure 16. Wind speed, direction and turbulent kinetic energy ~~profile~~ profile at tower 29/tse13 for SW winds.

towers 20/tse04 and 29/tse13 (Tables 6 and 8) on the hills depend on the dominant wind directions, showing the effects of the valley flow on the downstream hill. The effect of calculations on 20 m mesh ~~are minor. Here we can see again the limitations of the SRTM data, with RMSE higher than the cases based on either the military or the ALS data, 52% of the instances. And a threshold resolution around 20 and~~ compared to those on 40 m mesh are less than the effect of calculations on 40 m ~~, depending on the variable.~~ mesh compared to those on 80 m mesh.

6 Conclusions

Meshes for computational modelling of ~~flow~~ flow over the Perdigão site were created, based on three digital terrain models: high-resolution (2 m resolution) airborne lidar survey (ALS), Military (10 m) and SRTM (30 m) data. The mesh appraisal was carried out in two ways: by their ability to replicate the two main terrain attributes, elevation and slope, and by their effect on the wind ~~flow~~ flow computational results (wind speed, wind direction and turbulence kinetic energy) ~~.~~ at three locations.

Table 7. RMSE of wind speed, wind direction and turbulent kinetic energy for tower 20/tse04.

	W_{speed} (m/s)			Dir (°)			T.K.E (m^2/s^2)		
	SRTM	Mil	ALS	SRTM	Mil	ALS	SRTM	Mil	ALS
Southwesterly winds									
80	0.83	0.81	0.68	4.60	4.65	6.28	0.13	0.14	0.13
40	0.20	0.17	0.12	0.79	1.70	1.60	0.12	0.08	0.07
20	0.09	0.21	–	0.71	1.80	–	0.11	0.03	–
Northeasterly winds									
80	1.28	2.53	2.43	16.80	16.49	14.90	0.78	1.01	1.04
40	0.99	0.50	0.22	9.84	9.83	4.09	0.46	0.33	0.39
20	0.18	0.30	–	5.04	2.74	–	0.06	0.08	–

Table 8. RMSE of wind speed, wind direction and turbulent kinetic energy for tower 25/tse09.

	W_{speed} (m/s)			Dir (°)			T.K.E (m^2/s^2)		
	SRTM	Mil	ALS	SRTM	Mil	ALS	SRTM	Mil	ALS
Southwesterly winds									
80	0.87	0.77	0.69	26.67	20.10	14.81	0.33	0.29	0.26
40	0.92	0.90	0.70	38.14	75.35	48.96	0.36	0.34	0.16
20	0.81	0.84	-	37.03	92.73	-	0.36	0.32	-
Northeasterly winds									
80	2.82	3.67	3.54	157.07	158.04	153.56	0.25	0.49	0.49
40	0.39	0.88	0.53	88.82	79.37	69.95	0.51	0.33	0.23
20	0.19	0.17	–	40.61	43.20	–	0.22	0.15	–

About the digital terrain models, the main conclusions were the following:

1. The SRTM data is not an accurate representation of the Perdigão site.
2. Only meshes based on the ALS have the ability to reproduce the smaller scales between 10 and 100 m.
3. The ALS data yielded the lowest elevation errors; average RMSE around 5.8 m on 80 m, decreasing to 0.6 m on 10 m mesh.
4. The RMSE for SRTM ~~30 m~~ does not go below 7.4 m. A 40 m horizontal resolution based on the ALS data is enough to achieve an error below 1.4 m in ~~five~~ five key locations and below 0.28 m using a 20 m mesh.

Table 9. RMSE of wind speed, wind direction and turbulent kinetic energy for tower 29/tse13.

	W_{speed} (m/s)			Dir (°)			T.K.E (m^2/s^2)		
	SRTM	Mil	ALS	SRTM	Mil	ALS	SRTM	Mil	ALS
Southwesterly winds									
80	1.19	0.82	0.77	4.87	7.16	5.92	0.33	0.28	0.27
40	0.51	1.68	0.44	6.30	8.45	6.05	0.16	0.52	0.10
20	0.83	2.33	-	10.40	10.03	-	0.28	0.70	-
Northeasterly winds									
80	0.44	0.49	0.44	16.15	17.73	16.79	0.13	0.15	0.13
40	0.26	0.16	0.24	6.94	10.26	5.35	0.06	0.07	0.06
20	0.18	0.09	–	2.98	4.66	–	0.04	0.03	–

5. The maximum terrain slope was about $1.8\times$ higher ($-67.81°$) on a 20 m mesh resolution compared with an 80 m mesh resolution ($-37.33°$). An 80 m mesh does not accurately represent elevation and slope, mainly near the extreme elevation values (highs and lows).

The effect of the terrain model on the wind speed, wind direction and turbulent kinetic energy at three locations (SW ridge, valley and NW ridge) and two incoming wind directions (SW and NE) were the following:

1. In the case of SW winds, the mesh resolution effects on the ~~first~~ SW ridge were restricted to the ~~first~~ first 100 m a.g.l., where mesh ~~refinement~~ refinement decreased the wind speed and degraded the quantitative agreement with the experimental data, though replicating the ~~profile~~ profile shape.

2. Separated ~~flow field~~ flow field in the valley is perpendicular to the main ~~flow~~ flow direction. This region increases in height and length with the mesh ~~refinement~~refinement.

3. The ~~flow~~ flow (mainly the wind direction) in the valley was the most affected by terrain resolution; low velocities (about $1\,\mathrm{m\,s^{-1}}$) are associated with large variations of wind direction within the ~~first~~ first 150 m a.g.l..

Concerning the digital terrain models and meshes, the conclusions were the following.

1. It was found that 40 and 20 m meshes are resolutions –threshold resolution– beyond which no or ~~insignificant~~ insignificant changes occur both in terrain attributes, elevation and slope, and in the ~~flow field~~ flow field variables, wind speed, wind direction and turbulent kinetic energy.

2. ~~Furthermore, only~~ It is recommended that at least 40 and 20 m meshes based on military and ALS ~~are appropriate~~ be used to describe the Perdigão site~~and SRTM should be~~ , with SRTM restricted to far away regions.

3. ~~Meshes of at least 40 m horizontal resolution are recommended in computational modelling of the flow over Perdigão, and based on topography available from aerial survey.~~

Data availability. Three datafile types are available

~~**Lidar scanning files**~~

Lidar scanning files :

1. 5. Delivery information
   6.1 Coordinate system in plane and height: PT-TM06/ETRS89 / Altimetric Datum from Cascais
   6.2 File formats
   Laserdata: LAS 1.2
2. Ortho mosaic:
3. This delivery includes a lidar point cloud, and 5 cm and 20 cm orthophotos.

Topography data :

1. DTM of Perdigao site, terrain elevation on a regularly spaced $2\,\mathrm{m} \times 2\,\mathrm{m}$
2. Military map centred on Perdigão site, on a regularly spaced $10\,\mathrm{m} \times 10\,\mathrm{m}$
3. SRTM map centred on Perdigão site, on a regularly spaced $30\,\mathrm{m} \times 30\,\mathrm{m}$

Computational meshes :

1. Mesh 1: $20\,\mathrm{m} \times 20\,\mathrm{m}$
2. Mesh 2: $40\,\mathrm{m} \times 40\,\mathrm{m}$
3. Mesh 3: $80\,\mathrm{m} \times 80\,\mathrm{m}$

Author contributions. José M.L.M. Palma conceived, coordinated and was responsible for both the work and the manuscript writing. Carlos A.M. Silva carried out the fluid flow calculations, under the guidance of Vitor M.C. Gomes and Alexandre Silva Lopes. Teresa Simões and Paula Costa developed the algorithm for building identification. Vasco T.P. Batista contributed by processing the terrain data using the LAStools software.

Competing interests. No competing interests are present

Acknowledgements. The Perdigão-2017 field campaign was primarily funded by the US National Science Foundation, European Commission (ENER/FP7/618122/NEWA), Danish Energy Agency, German Federal Ministry of Economy and Energy, FCT-Portuguese Foundation for Science and Technology (NEWA/1/2014), and US Army Research Laboratory. We are grateful to the municipality of Vila Velha de

Ródão, landowners who authorized installation of ~~scientific~~ scientific equipment in their properties, the residents of Vale do Cobrão, Foz do Cobrão, Alvaiade, Chão das Servas and local businesses who kindly contributed to the success of the campaign. The campaign would not have been possible without the alliance of many persons and entities, too many to be listed here and to whom we are also grateful.

References

J. Alves. Perdigão terrestrial survey (tower 20/tse04). Technical report, Low Edge Consult Lda, Portugal, 4 2018. Terrestrial survey around tower 20/tse04, by Low Edge Consult Lda, under contract.

J. P. D. B. Carvalho. Stationarity periods during the Perdigão campaign. Master's thesis, Faculty of Engineering of the University of Porto, 2019. URL https://repositorio-aberto.up.pt/bitstream/10216/122036/2/348346.pdf.

F.A. Castro, J.M.L.M. Palma, and A. Silva Lopes. Simulation of the Askervein flow. Part 1: Reynolds averaged Navier-Stokes equations ($k-\varepsilon$ turbulence model). *Boundary-Layer Meteorology*, 107(3):501–530, June 2003. ISSN 0006-8314, 1573-1472. https://doi.org/10.1023/A:1022818327584. URL http://link.springer.com/article/10.1023/A%3A1022818327584.

Y. Deng, J. P. Wilson, and B. O. Bauer. DEM resolution dependencies of terrain attributes across a landscape. *International Journal of Geographical Information Science*, 21(2):187–213, January 2007. ISSN 1365-8816, 1362-3087. https://doi.org/10.1080/13658810600894364. URL http://www.tandfonline.com/doi/abs/10.1080/13658810600894364.

J.D. DeWitt, T.A. Warner, and J.F. Conley. Comparison of DEMS derived from USGS DLG, SRTM, a statewide photogrammetry program, ASTER GDEM and LiDAR: implications for change detection. *GIScience & Remote Sensing*, 52(2):179–197, March 2015. ISSN 1548-1603, 1943-7226. https://doi.org/10.1080/15481603.2015.1019708. URL http://www.tandfonline.com/doi/full/10.1080/15481603.2015.1019708.

DGT. ReNEP: The Portuguese Network of Continuously Operating Reference Stations Status, Products and Services (In Portuguese), 2017. URL http://renep.dgterritorio.gov.pt.

M. Diebold, C. Higgins, J. Fang, A. Bechmann, and M. B. Parlange. Flow over hills: A large-eddy simulation of the Bolund case. *Boundary-Layer Meteorology*, 148(1):177–194, July 2013. ISSN 0006-8314, 1573-1472. https://doi.org/10.1007/s10546-013-9807-0. URL http://link.springer.com/article/10.1007/s10546-013-9807-0.

ESRI. ArcGIS Desktop: Release 10.4. techreport, Environmental Systems Research Institute, Redlands, CA, February 2016.

T.G. Farr, P.A. Rosen, E. Caro, R. Crippen, R. Duren, S. Hensley, M. Kobrick, M. Paller, E. Rodriguez, L. Roth, D. Seal, S. Shaffer, J. Shimada, J. Umland, M. Werner, M. Oskin, D. Burbank, and D. Alsdorf. The Shuttle Radar Topography Mission. *Reviews of Geophysics*, 45(2), June 2007. ISSN 1944-9208. https://doi.org/10.1029/2005RG000183. URL https://agupubs.onlinelibrary.wiley.com/doi/abs/10.1029/2005RG000183.

H. J. S. Fernando, J. Mann, J.M.L.M. Palma, J. K. Lundquist, R. J. Barthelmie, M. Belo-Pereira, W. O. J. Brown, F. K. Chow, T. Gerz, C. M. Hocut, P. M. Klein, L. S. Leo, J. C. Matos, S. P. Oncley, S. C. Pryor, L. Bariteau, T. M. Bell, N. Bodini, M. B. Carney, M. S. Courtney, E. D. Creegan, R. Dimitrova, S. Gomes, M. Hagen, J. O. Hyde, S. Kigle, R. Krishnamurthy, J. C. Lopes, L. Mazzaro, J. M. T. Neher, R. Menke, P. Murphy, L. Oswald, S. Otarola-Bustos, A. K. Pattantyus, C. Veiga Rodrigues, A. Schady, N. Sirin, S. Spuler, E. Svensson, J. Tomaszewski, D. D. Turner, L. van Veen, N. Vasiljević, D. Vassallo, S. Voss, N. Wildmann, and Y. Wang. The Perdigão: Peering into microscale details of mountain winds. *Bulletin of the American Meteorological Society*, 100(5):799–819, May 2019. ISSN 0003-0007, 1520-0477. https://doi.org/10.1175/BAMS-D-17-0227.1. URL http://journals.ametsoc.org/doi/10.1175/BAMS-D-17-0227.1.

I.V. Florinsky and G.A. Kuryakova. Determination of grid size for digital terrain modelling in landscape investigations—exemplified by soil moisture distribution at a micro-scale. *International Journal of Geographical Information Science*, 14(8):815–832, December 2000. ISSN 1365-8816. https://doi.org/10.1080/136588100750022804. URL https://doi.org/10.1080/136588100750022804.

V. M. M. G. C. Gomes and J. M. L. M. Palma. Computational modelling of a large dimension wind farm cluster using domain coupling. *Journal of Physics: Conference Series*, 753(8):082032, 2016. URL http://stacks.iop.org/1742-6596/753/i=8/a=082032.

V.M.M.G. Costa Gomes, J.M.L.M. Palma, and A. Silva Lopes. Improving actuator disk wake model. *Journal of Physics: Conference Series*, 524(1):012170, June 2014. ISSN 1742-6596. https://doi.org/10.1088/1742-6596/524/1/012170. URL http://iopscience.iop.org/1742-6596/524/1/012170.

L. Hawker, P. Bates, J. Neal, and J. Rougier. Perspectives on digital elevation model (DEM) simulation for flood modeling in the absence of a high-accuracy open access global dem. *Frontiers in Earth Science*, 6, 2018. ISSN 2296-6463. https://doi.org/10.3389/feart.2018.00233. URL https://www.frontiersin.org/articles/10.3389/feart.2018.00233/full. Publisher: Frontiers.

J. Lange, J. Mann, J. Berg, D. Parvu, R. Kilpatrick, A. Costache, J. Chowdhury, K. Siddiqui, and H. Hangan. For wind turbines in complex terrain, the devil is in the detail. *Environmental Research Letters*, 12(9):094020, 2017. ISSN 1748-9326. https://doi.org/10.1088/1748-9326/aa81db. URL http://stacks.iop.org/1748-9326/12/i=9/a=094020.

LAStools. Efficient LiDAR processing software (version 190927, academic), 2019. URL http://rapidlasso.com.

J. C. Lopes da Costa, F.A. Castro, J.M.L.M. Palma, and P. Stuart. Computer simulation of atmospheric flows over real forests for wind energy resource evaluation. *Journal of Wind Engineering and Industrial Aerodynamics*, 94:603–620, 2006. https://doi.org/10.1016/j.jweia.2006.02.002. URL https://www.sciencedirect.com/science/article/pii/S0167610506000328.

R. Mahalingam and M. J. Olsen. Evaluation of the influence of source and spatial resolution of DEMs on derivative products used in landslide mapping. *Geomatics, Natural Hazards and Risk*, 7(6):1835–1855, November 2016. ISSN 1947-5705. https://doi.org/10.1080/19475705.2015.1115431. URL https://doi.org/10.1080/19475705.2015.1115431.

C. Mallet and F. Bretar. Full-waveform topographic lidar: State-of-the-art. *ISPRS Journal of Photogrammetry and Remote Sensing*, 64 (1):1–16, January 2009. ISSN 0924-2716. https://doi.org/10.1016/j.isprsjprs.2008.09.007. URL http://www.sciencedirect.com/science/article/pii/S0924271608000993.

B.B. Mandelbrot. How long is the coast of Britain? statistical self-similariry and fractional dimension. *Science*, 156:636–638, 1967. https://doi.org/10.1126/science.156.3775.636.

B.B. Mandelbrot. *The Fractal Geometry of Nature*. W.H. Freeman and Company, New York, updated edition, 1982. ISBN 0-7167-1186-9.

J. Mann, N. Angelou, J. Arnqvist, D. Callies, E. Cantero, R. Chávez Arroyo, M. Courtney, J. Cuxart, E. Dellwik, J. Gottschall, S. Ivanell, P. Kuhn, G. Lea, J. Matos, C. Rodrigues, J. Palma, L. Pauscher, A. Peña, J. Rodrigo, S. Söderberg, and N. Vasiljević. Complex terrain experiments in the new european wind atlas. *Philosophical Transactions of the Royal Society A: Mathematical Physical and Engineering Sciences*, 375:(2091):20160101, April 2017. https://doi.org/10.1098/rsta.2016.0101. URL http://rsta.royalsocietypublishing.org/content/375/2091/20160101.

R. Menke, N. Vasiljević, J. Mann, and J. K. Lundquist. Characterization of flow recirculation zones at the Perdigão site using multi-lidar measurements. *Atmospheric Chemistry and Physics*, 19(4):2713–2723, March 2019. ISSN 1680-7316. https://doi.org/10.5194/acp-19-2713-2019. URL https://www.atmos-chem-phys.net/19/2713/2019/.

N. G. Mortensen, L. Landberg, I. Troen, E. L. Petersen, O. Rathmann, and M. Nielsen. WAsP utility programs. Technical Report Risø-R-995(EN), Risø National Laboratory, Roskilde, Denmark, September 2004. URL http://orbit.dtu.dk/files/106312446/ris_i_2261.pdf.

S. Mukherjee, P. K. Joshi, S. Mukherjee, A. Ghosh, R. D. Garg, and A. Mukhopadhyay. Evaluation of vertical accuracy of open source Digital Elevation Model (DEM). *International Journal of Applied Earth Observation and Geoinformation*, 21:205–217, April 2013. ISSN 0303-2434. https://doi.org/10.1016/j.jag.2012.09.004. URL http://www.sciencedirect.com/science/article/pii/S030324341200195X.

V. Nikora and D. Goring. Mars topography: bulk statistics and spectral scaling. *Chaos, Solitons & Fractals*, 19(2):427 – 439, 2004. ISSN 0960-0779. https://doi.org/10.1016/S0960-0779(03)00054-7. URL http://www.sciencedirect.com/science/article/pii/S0960077903000547. Fractals in Geophysics.

NIRAS. Perdigão aerial survey. Technical report, NIRAS, 4 2015. This is a report of a helicopter airborne survey delivered by NIRAS with assistance from Blom TopEye in order to produce data for digital elevation model and ortho photo. This delivery includes a LiDAR point cloud, and 5cm (plus 20cm) Ortho Photo.

J.M.L.M. Palma, F.A. Castro, L.F. Ribeiro, A.H. Rodrigues, and A.P. Pinto. Linear and nonlinear models in wind resource assessment and wind turbine micro-siting in complex terrain. *Journal of Wind Engineering and Industrial Aerodynamics*, 96:2308–2326, December 2008. https://doi.org/10.1016/j.jweia.2008.03.012. URL http://www.sciencedirect.com/science/article/pii/S0167610508001037.

J.M.L.M. Palma, R. Menke, J. Mann, S. Oncley, J. Matos, and A. Silva Lopes. Perdigão–2017: experiment layout (Version 1). Technical report, *NEWA: New European Wind Atlas* (FCT Project number NEWA/0001/2014), August 23 2018. URL https://perdigao.fe.up.pt/experiments/3/documents/1232. Project coordinator: Danmarks Tekniske Universitet (DTU Wind).

J.M.L.M. Palma, A. Silva Lopes, V.M. Costa Gomes, C. Veiga Rodrigues, R. Menke, N. Vasiljević, and J. Mann. Unravelling the wind flow over highly complex regions through computational modeling and two-dimensional lidar scanning. *Journal of Physics: Conference Series*, 1222:012006, May 2019. ISSN 1742-6588, 1742-6596. https://doi.org/10.1088/1742-6596/1222/1/012006. URL https://iopscience.iop.org/article/10.1088/1742-6596/1222/1/012006.

P. J. Roache. *Verification and Validation in Computational Science and Engineering*. Hermosa Publishers, Albuquerque, USA, 1998. ISBN 0-913478-08-3.

J. T. S. Savage, P. Bates, J. Freer, J. Neal, and G. Aronica. When does spatial resolution become spurious in probabilistic flood inundation predictions? *Hydrological Processes*, 30(13):2014–2032, June 2016. ISSN 0885-6087. https://doi.org/10.1002/hyp.10749. URL https://onlinelibrary.wiley.com/doi/full/10.1002/hyp.10749. Publisher: John Wiley & Sons, Ltd.

R. Sibson. A brief description of natural neighbor interpolation. pages 21–36, June 1981. In *Interpreting Multivariate Data*, V. Barnett (Editor), John Wiley and Sons, New York,.

C.A.M. Silva. Computational study of atmospheric flows over Perdigão: terrain resolution and domain size. Master's thesis, Faculty of Engineering of the University of Porto, 2018. URL https://hdl.handle.net/10216/113854.

A.L. Simpson, S. Balog, D. K. Moller, B. Strauss, and K. Saito. An urgent case for higher resolution digital elevation models in the world's poorest and most vulnerable countries. *Frontiers in Earth Science*, 3, 2015. ISSN 2296-6463. https://doi.org/10.3389/feart.2015.00050. URL https://www.frontiersin.org/articles/10.3389/feart.2015.00050/full. Publisher: Frontiers.

R. B. Stull. *An Introduction to Boundary Layer Meteorology*. Kluwer Academic Publishers, 1988.

UCAR/NCAR-EOL. NCAR/EOL quality controlled 5-minute ISFS surface flux data, geographic coordinate, tilt corrected, 2019. URL https://data.eol.ucar.edu/dataset/536.011.

N. Vasiljević, J.M.L.M. Palma, N. Angelou, J.C. Matos, R. Menke, G. Lea, J. Mann, M. Courtney, L. Frölen Ribeiro, and V. M. M. G. C. Gomes. Perdigão 2015: methodology for atmospheric multi-Doppler lidar experiments. *Atmos. Meas. Tech.*, 10(9):3463–3483, September 2017. ISSN 1867-8548. https://doi.org/10.5194/amt-10-3463-2017. URL https://www.atmos-meas-tech.net/10/3463/2017/.

J Wagner, T Gerz, N Wildmann, and K Gramitzky. Long-term simulation of the boundary layer flow over the double-ridge site during the Perdigão 2017 field campaign. *Atmospheric Chemistry and Physics*, 19(2):1129–1146, January 2019. ISSN 1680-7316. https://doi.org/10.5194/acp-19-1129-2019. URL https://www.atmos-chem-phys.net/19/1129/2019/acp-19-1129-2019-discussion.html.

D. Watson. *Nngride: An Implementation of Natural Neighbor Interpolation*. David Watson, P.O. Box 734, Claremont, WA 6010, Australia. edition, 1994.

S. Wise. Assessing the quality for hydrological applications of digital elevation models derived from contours. *Hydrological Processes*, 14(11-12):1909–1929, 2000. ISSN 1099-1085. https://doi.org/10.1002/1099-1085(20000815/30)14:11/12<1909::AID-

HYP45>3.0.CO;2-6. URL https://onlinelibrary.wiley.com/doi/abs/10.1002/1099-1085%2820000815/30%2914%3A11/12%3C1909%3A%3AAID-HYP45%3E3.0.CO%3B2-6. _eprint: https://onlinelibrary.wiley.com/doi/pdf/10.1002/1099-1085%2820000815/30%2914%3A11/12%3C1909%3A%3AAID-HYP45%3E3.0.CO%3B2-6.

N. Wood. The onset of separation in neutral, turbulent flow over hills. *Boundary-Layer Meteorology*, 76(1-2):137–164, 1995. ISSN 0006-8314. https://doi.org/10.1007/BF00710894. URL http://www.springerlink.com/content/v2412rh223072568/.

Y. Yamaguchi, A.B. Kahle, H. Tsu, T. Kawakami, and M. Pniel. Overview of Advanced Spaceborne Thermal Emission and Reflection Radiometer (ASTER). *IEEE Transactions on Geoscience and Remote Sensing*, 36(4):1062–1071, July 1998. ISSN 01962892. https://doi.org/10.1109/36.700991. URL http://ieeexplore.ieee.org/document/700991/.

W. Zhang and D. R. Montgomery. Digital elevation model grid size, landscape representation, and hydrologic simulations. *Water Resources Research*, 30(4):1019–1028, April 1994. ISSN 00431397. https://doi.org/10.1029/93WR03553. URL http://doi.wiley.com/10.1029/93WR03553.